JCI The Journal of Clinical Investigation

L-2-hydroxyglutarate remodeling of the epigenome and epitranscriptome creates a metabolic vulnerability in kidney cancer models

Anirban Kundu, … , Jason M. Tennessen, Sunil Sudarshan

J Clin Invest. 2024. https://doi.org/10.1172/JCI171294.

Research In-Press Preview Metabolism Oncology

Graphical abstract

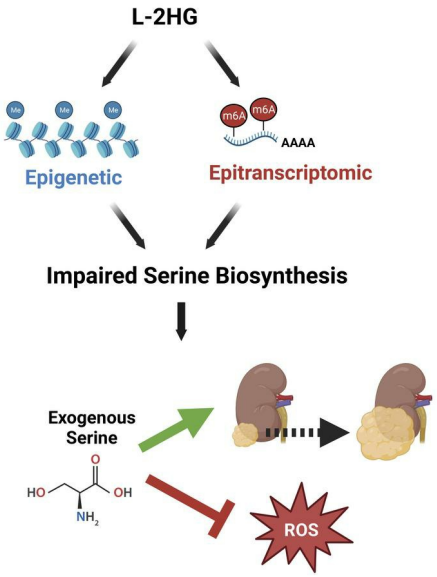

L-2-hydroxyglutarate remodeling of the epigenome and epitranscriptome creates a metabolic vulnerability in kidney cancer models

Anirban Kundu[#, 1, 9], Garrett J. Brinkley[#,1], Hyeyoung Nam[1], Suman Karki[1], Richard Kirkman[1], Madhuparna Pandit[1], EunHee Shim[1], Hayley Widden[2], Juan Liu[3], Yasaman Heidarian[4], Nader H. Mahmoudzadeh[4], Alexander J. Fitt[4], Devin Absher[5], Han-Fei Ding[6], David K. Crossman[7], William J. Placzek[2], Jason W. Locasale[3], Dinesh Rakheja[8], Jonathan E. McConathy[9], Rekha Ramachandran[10], Sejong Bae[10], Jason M. Tennessen[4], Sunil Sudarshan*[, 1]

[#] Equal contribution.

Departments of [1] Urology, [2] Biochemistry & Molecular Genetics, [6] Pathology, [7]Genetics, [9]Radiology, and [10]MedicineUniversity of Alabama at Birmingham, AL

[3] Department of Pharmacology and Cancer Biology, Duke University School of Medicine, Durham, NC

[4] Department of Biology, Indiana University, Bloomington, IN

[5] HudsonAlpha Institute for Biotechnology, Huntsville, AL (current: Kaiser Permanente Research Bank, Oakland, CA)

[8] Department of Pathology, University of Texas Southwestern Medical Center, Dallas, TX

[9] Department of Urology, University of Arizona, Tuscon, AZ (current)

* Corresponding Author

*Correspondence: ssudarshan@uabmc.edu

1105 Faculty Office Tower

510 20th Street South

Birmingham, AL 35294

205-996-8765 Office

205-934-4933 Fax

Conflict of Interest Statement: The authors have declared that no conflict of interest exists

Abstract

Tumor cells are known to undergo considerable metabolic reprogramming to meet their unique demands and drive tumor growth. At the same time, this reprogramming may come at a cost with resultant metabolic vulnerabilities. The small molecule L-2-hdroxyglutarate (L-2HG) is elevated in the most common histology of renal cancer. Similar to other oncometabolites, L-2HG has the potential to profoundly impact gene expression. Here, we demonstrate that L-2HG remodels amino acid metabolism in renal cancer cells through the combined effects on histone methylation and RNA N^6-methyladenosine (m6A). The combined effects of L-2HG result in a metabolic liability that renders tumors cells reliant on exogenous serine to support proliferation, redox homeostasis, and tumor growth. In concert with these data, high L-2HG kidney cancers demonstrates reduced expression of multiple serine biosynthetic enzymes. Collectively, our data indicate that high L-2HG renal tumors could be specifically targeted by strategies that limit serine availability to tumors.

Keywords: Cancer Metabolism, kidney cancer, oncometabolite, epigenome, epitranscriptome, RNA methylation, serine biosynthesis

Introduction

Oncometabolites are small molecules that aberrantly accumulate within tumor cells. These small molecules can have either tumor promoting or suppressive effects indicating that their impact on tumor biology is highly context dependent. Oncometabolites have been identified in multiple subtypes of renal cell carcinoma (RCC) including fumarate and succinate which are due to loss of function mutations for the genes encoding fumarate hydratase (*FH)* and succinate dehydrogenase (*SDHB, SDHC, SDHD*), respectively(1). Elevations of (D) 2-hydroxyglutarate have been identified in other tumor types in the context of isocitrate dehydrogenase (*IDH1/2*) mutations(2-4). We previously reported elevations of (L) 2-hydroxyglutarate (L-2HG) in the most common histology of kidney cancer referred to as clear cell renal cell carcinoma (ccRCC)(5). A shared feature of the oncometabolites described to date is their structural similarity with α-ketoglutarate. α-KG is a cofactor for enzymes that catalyze both histone and nucleotide modifications. Prior studies have indicated that the biologically relevant target(s) of oncometabolites are enzymes that require α-KG, either as a substrate or a cofactor(6-11). Deciphering the relevant target(s) of an oncometabolite and the ensuing impact on tumor biology could inform novel treatment strategies.

L-2HG accumulates in RCC due to loss of the enzyme L-2HG dehydrogenase (L2HGDH). We previously identified that approximately 25% of primary ccRCCs have excessively high L-2HG levels (≥20-fold elevation) with further increases in metastatic tissue deposits(5, 12). L-2HG promotes tumor growth in xenograft models. These data provide compelling rationale to delineate L-2HG's target(s) in RCC which could inform novel approaches to treat L-2HG driven tumors. We therefore undertook unbiased approaches to study L-2HG's impact on tumor biology. Our studies identified L-2HG remodels tumor metabolism through combined effects on both the epigenome and epitranscriptome. These effects lead to a metabolic liability resulting in dependence on exogenous serine to support proliferation, redox homeostasis, and tumor growth. While strategies to target serine availability have been proposed, a major gap is which tumors are most likely to respond to such strategies and insight into the mechanisms that promote this sensitivity. Our data reveal a potential oncometabolic biomarker

in elevated L-2HG that could inform precision-based approaches that target metabolism for the most common variant of kidney cancer.

RESULTS

L-2HG suppresses mRNA expression of amino acid metabolism genes.

To assess L-2HG's impact on RCC biology in an unbiased manner, we performed RNAseq analysis of a paired cell line system. We previously noted that RXF-393 RCC cells have reduced expression of L2HGDH enzyme with a concomitant increase in cellular L-2HG levels(5). We stably transduced these cells with control vector and L2HGDH cDNA to perform a comparative analysis between high and low L-2HG cells. We observed that restoring L2HGDH (i.e. lowering L-2HG levels) resulted in the increased expression of mRNAs related to amino acid metabolism including biosynthetic enzymes and metabolite transporters (Fig 1A and supplemental Table S1). Among the most significantly increased mRNAs upon L2HGDH restoration were those encoding for phosphoglycerate dehydrogenase (*PHGDH*) and phosphoserine aminotransferase 1 (*PSAT1*). PHGDH and PSAT1 catalyze the first two of three steps of *de novo* serine biosynthesis. Accordingly, pathway analysis of RNAseq data demonstrated an enrichment of genes related to serine/glycine metabolism upon lowering L-2HG levels (supplemental Figure S1A-B). We validated these data via real time RT-qPCR (Figure 1B). We next determined if L2HGDH's catalytic activity was required for this effect using a cDNA encoding a patient-derived mutant of L2HGDH (A241G). RCC cells transduced with WT L2HGDH demonstrate a prominent reduction in L-2HG levels whereas the A241G mutant has only a modest effect on L-2HG levels (supplemental Figure S1C). In multiple lines tested, we found that L2HGDH's catalytic activity was required to increase mRNA expression of amino acid biosynthetic and transporter genes (Figure 1C-D). We next determined the impact of restoring L2HGDH on protein levels of amino acid biosynthetic enzymes. In both 769p and 786-O RCC cells, restoring L2HGDH led to increased expression of both PHGDH and PSAT1 protein (Figure 1E). In addition, L2HGDH restoration led to increased levels of asparagine synthase (ASNS) (Figure 1F). In alignment with the mRNA data, L2HGDH's catalytic activity was required for the induction of PHGDH and PSAT1 protein levels in RCC cells (Figure 1G-H). Based on these data, we utilized CRISPR/Cas9 to knockout L2HGDH expression

in HK-2 immortalized renal epithelial cells which have high L2HGDH enzyme expression and low basal L-2HG levels(5). *L2HGDH* knockout cells demonstrated increased L-2HG levels without any significant increase in D-2HG (Figure 1I). Consistent with our gain of function studies, *L2HGDH* knockout led reduced mRNA levels of amino acid biosynthetic genes (Figure 1J). Furthermore, rescue via transient transfection of knockout cells with L2HGDH cDNA led to increased PHGDH and PSAT1 protein (supplemental Figure S1D). We next determined if exogenous L-2HG could have similar effects. We therefore treated cells with an esterified for L-2HG (octyl-ester) which raises intracellular levels of L-2HG(5). Consistent with our gain/loss of function studies with L2HGDH, exogenous L-2HG led to reduced expression of PHGDH (Figure 1K, compare first two lanes). Given these findings, we considered if L-2HG's effects could be through inhibition of α-ketoglutarate (α-KG) dependent dioxygenases. As an initial approach, we utilized dimethyloxalylglycine (DMOG). Due to structural similarity with α-KG, DMOG can competitively inhibit α-ketoglutarate dependent dioxygenases. Similar to exogenous L-2HG, DMOG treatment also reduced PHGDH expression in HK-2 renal epithelial cells (Figure 1K, last lane).

L-2HG suppresses ATF4 expression.

Our finding that raised cellular L-2HG levels resulted in suppressed expression of amino acid biosynthetic genes led us to consider effects on activating transcription factor 4 (ATF4). ATF4 is a master regulator of amino acid metabolism genes and coordinates the cellular response to nutrient stress. Similar to our findings with amino acid biosynthetic enzymes, L2HGDH restoration led to increased ATF4 protein in multiple RCC lines examined (Figure 2A). Furthermore, this effect was dependent on L2HGDH catalytic activity as mutant enzyme did not promote ATF4 protein expression (Figure 2B). Consistent with these data, L2HGDH knockout renal epithelial cells demonstrated reduced ATF4 expression (Figure 2C). Given these data, we considered if L-2HG suppression of amino acid biosynthetic enzymes could, at least in part, be due to suppression of ATF4. In support, we find that expression of ATF4 cDNA in high L-2HG RCC cells promotes expression of PHGDH, an established target gene of ATF4 (Figure 2D). These data prompted us to examine effects on *ATF4* transcript levels. Lowering L-2HG levels in RCC cells via L2HGDH restoration led to increased *ATF4* mRNA

levels in 769p and 786-O RCC cells (Figure 2E). As these data supported an epigenetic basis for L-2HG's effect on amino acid metabolism, we considered α-KG requiring enzymes implicated in the regulation of amino acid metabolism. The histone lysine demethylase KDMC4 promotes that mRNA expression of amino acid metabolism genes involved in both biosynthesis and transport(13). KDM4C removes the histone repressive mark H3 lysine 9 trimethylation (H3K9me3) at the *ATF4* mRNA. Furthermore, KDM4C physically interacts with ATF4 protein to promote expression of serine biosynthetic genes including *PHGDH* and *PSAT1.* However, KDM4C's ability to regulate amino acid metabolism in the setting of an oncometabolite has not been considered. L2HGDH restoration had no effect on KDM4C expression (supplemental Figure S2A). We attempted a rescue experiment by ablating KDM4C in L2HGDH-restored cells. Using an siRNA pool, KDM4C knockdown resulted in reduced ATF4 with reduced *PHGDH* mRNA (supplemental Figure S2B-C). Similarly, KDM4C knockdown with multiple individual siRNA constructs in L2HGDH restored RCC cells led to reduced ATF4 protein along with reduced expression of serine biosynthetic enzyme PHGDH and PSAT1 (Figure 2F-G). These rescue data support that L-2HG's suppression of ATF4/PHGDH/PSAT1 is mediated in part through KDM4C inhibition.

A major mode of regulation for ATF4 is at the level of mRNA translation. The *ATF4* mRNA has multiple upstream open reading frames (uORFs) in the 5' untranslated region. Under nutrient replete conditions, the ATF4 transcript is poorly translated due to translation of uORFs which are overlapping and out of frame with the ATF4 open reading frame start codon(14, 15). Under stresses such as nutrient starvation, "leaky" scanning by ribosomes allows ATF4 translation within the correct reading frame which increases ATF4 protein(16). We therefore considered L-2HG's impact on translation of the *ATF4* mRNA using a luciferase-based reporter construct(17). We observed that WT L2HGDH led to increased ATF4 translation in both 769p and 786-O RCC cells (Figure 2H). In contrast, mutant L2HGDH did not increase ATF4 translation. Zhou *et al.* recently reported that RNA N^6-methylation of adenosine (m^6A) in the *ATF4* mRNA can impede translation of the open reading frame that produces ATF4 protein(18). The m6A mark is reversible. The mark is laid down by an RNA methyltransferase complex(19). In contrast, m6A can be removed by the RNA demethylases ALKBH5 and FTO(20, 21).

As both ALKBH and FTO require α–KG as a cofactor for demethylase activity, we considered whether L-2HG could impact the expression of amino acid metabolism factors through RNA methylation.

L-2HG promotes mRNA m6A methylation.

We therefore first examined the impact of raised L-2HG in RCC on global mRNA m6A levels via dot blot assay using an antibody specific to the m6A mark. Lowering L-2HG levels via L2HGDH restoration led to a significant reduction in mRNA m6A levels in multiple lines tested (Figure 3A-C). As an orthogonal approach, we measured m6A levels via LC-MS which also demonstrated that L2HGDH lowers m6A levels (Figure 3D). Furthermore, this effect depends on L2HGDH's catalytic activity as the A241G mutant did not lower m6A levels in RCC cells (Figure 3E). L-2HG has previously been shown to inhibit the enzymatic activity of FTO. We therefore examined L-2HG's effects on the activity of recombinant ALKBH5 on a methylated RNA substrate. As demonstrated in the Figure 3F, L-2HG inhibits ALKBH5 activity in a dose-dependent manner. We next considered if L2HGDH's lowering of m6A was mediated through ALKBH5 and/or FTO. As demonstrated in Figure 3G, ablation of either FTO or ALKBH5 increased m6A levels in 786-O cells expressing L2HGDH. Given these data, we performed transcriptome-wide profiling of RNA methylation (m6A-seq) in high L-2HG (control vector) RCC cells with low L-2HG (L2HGDH restored) cells. As compared with dot blot, this analysis can determine the location and intensity of m6A peaks in mRNA. m6A-seq of high (control vector) vs low L-2HG (L2HGDH restored) cells demonstrates that L-2HG promotes a marked increase in m6A peaks throughout the transcriptome (Figure 3H and supplemental Table S2). The predominant location of this increase is located with the 3'UTR of mRNAs consistent with where m6A is most commonly located within transcripts (supplemental Figure 3A). We did not find a significant effect of L-2HG on m6A on the ATF4 mRNA (data not shown). However, L-2HG does promote m6A accumulation within the 3'UTR of the transcript for *PSAT1* which encodes the enzyme that catalyzes the second reaction of serine biosynthesis (Figure 3I). m6A immunoprecipitation followed by RT-qPCR in multiple RCC lines demonstrated that L-2HG promotes m6A accumulation in the 3'UTR of *PSAT1* mRNA (Figure 3J and supplemental Figure S3B).

L-2HG suppresses PSAT1 expression through mRNA m6A.

We next sought to determine the role of L-2HG induced m6A in regulating PSAT1 expression. We therefore knocked down METTL3 which is the catalytic subunit of the m6A methyltransferase complex. METTL3 knockdown led to increased PSAT1 protein expression (Figure 4A-B). As expected, METTL3 knockdown led to reduced mRNA m6A levels (supplemental Figure S3A-B). Although METTL3 knockdown trended toward a slight increase in *PSAT1* mRNA levels, these data did not reach statistical significance (Figure 4C). Given these data, we next determined if RNA m6A demethylases can regulate PSAT1 expression. In HK-2 renal epithelial cells which have low basal L-2HG levels, knockdown of the m6A demethylase ALKBH5 led to reduced PSAT1 (Figure 4D). L2HGDH restoration in high L-2HG increased PSAT1 levels. We determined if this effect could be rescued by m6A demethylase ablation via either ALKBH5 or FTO knockdown. In both 786-O L2HGDH and 769-P L2HGDH cells, ALKBH5 knockdown led to reduced PSAT1 (similar to high L-2HG cells) (Figure 4E-F). Furthermore, FTO knockdown also reduced PSAT1 in 769p L2HGDH cells (Figure 4G). m6A methylation occurs on DR<u>A</u>CH motifs (D=G/A/U; R=G/A; H=A/U/C; central A is methylated). The most common sequence for this motif is GGACT. Notably, the 3'UTR of *PSAT1* has a single GGACT site (supplemental Figure S4C). Single nucleotide resolution mapping of m6A in HEK293 cells by Linder *et al.* using both CIMS (crosslink induced mutational sites) and CITS (crosslink induced truncation sites) identified m6A at this site (supplemental Figure S4D)(22). As m6A IP has a resolution of 100-200 base pairs, we used SELECT for single nucleotide resolution of m6A levels(23). SELECT is based on the premise that m6A (as opposed to unmodified adenosine) hinders both *Bst1* DNA polymerase elongation and *SplintR* nick ligase activity. Oligos are designed that are immediately upstream and downstream of the RNA m6A site. The oligos have PCR adapters which allows for quantification with qPCR. Sites with higher m6A levels are amplified less efficiently. METTL3 knockdown in high L-2HG RCC cells led to reduced m6A levels at the GG**A**CT site within the *PSAT1* 3'UTR (Figure 4H). We then determined the impact of L2HGDH restoration on m6A levels at this site. In multiple RCC lines, L2HGDH restoration (i.e. lowering L-2HG levels) resulted in significantly reduced m6A levels at this site (Figure 4I-J). We next determined the significance of this methylation with regard to PSAT1 expression. We therefore generated a *PSAT1* cDNA construct which contained the 3'UTR and stably expressed this construct in high L-2HG RCC cells. Constructs included an N-terminus FLAG tag to

differentiate from endogenous PSAT1. Similar to endogenous PSAT1, knockdown of m6A methyltransferase subunit METTL3 led to increased expression of tagged PSAT1 (Figure 4K-L). In tandem, we expressed a *PSAT1* mutant in which the GG**A**CT site in the 3'UTR is mutated to GG**T**CT (PSAT1 Mut). In contrast to WT, mutant PSAT1 levels did not change with METTL3 ablation (Figure 4M). Collectively, these data demonstrate that L-2HG promotes m6A methylation in the 3'UTR of *PSAT1* mRNA which results in lower expression of this serine biosynthetic enzyme.

L-2HG promotes a serine liability in RCC.

Given that L-2HG suppressed the expression of serine biosynthetic enzymes, we next assessed the sequalae of this finding. The starting substrate for *de novo* serine biosynthesis is the glycolytic intermediate 3-phosphoglycerate. We therefore utilized fully labeled 13C glucose [U-^{13}C] with LC-MS to assess serine biosynthesis as a function of L-2HG. L2HGDH restoration in RCC cells resulted in enhanced *de novo* serine biosynthesis as determined by increased production of fully labelled (m+3) serine (Figure 5A and supplemental Table S3). In addition, we found that L2HGDH led to increased levels of the m+2 isotopologue of serine (Figure S5A) which can be generated via the interconversion of serine and glycine via serine hydroxymethyltransferases (SHMTs). As these data indicate that serine biosynthesis is reduced in the setting of raised L-2HG, we next considered the effects of serine availability on the growth of RCC cells as a function of L-2HG status. We therefore assessed proliferation in the presence/absence of serine and glycine (Ser/Gly). Glycine is also modulated as it can be converted to serine by SHMTs as noted above. The proliferation of control OS-RC-2 cells (high L-2HG) was significantly reduced upon depletion of ser/gly from the media (Figure5B). These effects were sustained in multiple high L-2HG RCC lines cultured for a longer period (supplemental Figure S5B). Consistent with prior studies, L2HGDH restoration led to reduced proliferation. However, the proliferation of L2HGDH restored OS-RC-2 cells was not impacted by ser/gly depletion from the media (Figure5B-C). Similarly, in other RCC lines tested, the effect of ser/gly deprivation on proliferation was significantly greater in control (high L-2HG) cells as compared with L2HGDH restored (low L-2HG) cells (Figure 5D and S5B-C). Expression of *PHGDH* cDNA in high L-2HG RCC cells could rescue the ability of cells to proliferate in the absence of serine in the media (Figure5E-G). We next performed loss of

function studies in SN12PM6 RCC cells which have retained L2HGDH expression. Knockdown of L2HGDH expression in these cells led to reduced expression of PHGDH (Figure 5H) and the expected increase in cellular L-2HG levels (Figure 5I). The proliferation of control vector transduced cells was not impacted by ser/gly deprivation (Figure 5J). In contrast, the proliferation of L2HGDH knockdown cells is reduced with ser/gly deprivation (Figure 5K). Correspondingly, knockdown of PHGDH in SN12PM6 cells renders proliferation sensitive to ser/gly deprivation (Figure S5D-E). In agreement, the proliferation of L2HGDH restored RCC cells in media lacking ser/gly was reduced with PSAT1 knockdown (supplemental Figure S5G-H).

Given these in vitro data, we next considered the effects of limiting serine availability to the growth of high L-2HG RCC in vivo given the reliance of tumor cells on exogenous serine to maintain proliferation. A potential source of serine is through the diet. We therefore considered the effects of ser/gly depletion from the diet on the growth of high L-2HG RCC xenografts. Mice were stratified to receive chow +/- ser/gly at the time of subcutaneous injection of OS-RC-2 cells. In mice fed chow without ser/gly, tumor xenograft growth was delayed (Figure 5O-left panel). Furthermore, end of study xenograft tumor size was significantly lower in mice fed chow lacking ser/gly (Figure 5O-right panel). As a complementary approach, we initially injected 786-O cells in mice fed normal chow and allowed xenografts to establish. Mice were then stratified to receive chow +/- ser/gly. Further xenograft growth was largely blocked in mice who were switched to a diet lacking ser/gly (Figure 5P-left panel) with significantly smaller xenograft size at end of study (Figure 5P-right panel).

Exogenous serine is required for glutathione synthesis in high L-2HG RCC.

Based on these data, we considered serine's contribution to tumor biology using steady-state metabolomics by comparing high L-2HG RCC cells cultured with media under the following conditions: a) with ser/gly, b) without ser/gly, and c) glycine alone. As demonstrated by principal component analysis (PCA), the metabolomes of cells cultured with ser/gly were distinct from the other culture conditions (Figure 6A). High L-2HG 769p RCC cells cultured in the presence of ser/gly had significantly higher steady state levels of glutathione (GSH) as well as metabolites derived from GSH including glutathione disulfide (GSSG) and L-cysteinylglycine (Figure 6B and supplemental Table S4). These

data are particularly relevant as GSH is among the most enriched metabolites in RCC as compared with normal kidney (over 100-fold) in multiple metabolomic data sets(24, 25). GSH is a tripeptide consisting of the amino acids glutamate, cysteine, and glycine. Serine can directly contribute to GSH through its conversion to glycine via SHMTs. Glutathione synthase condenses glycine and γ-glutamylcysteine to form GSH (Figure 6C - red arrow). Alternatively, serine can directly contribute to cysteine pools via transsulfuration which can then be incorporated into glutathione (Figure 6C - green arrow). Exogenous serine alone was able to maintain glutathione pools similar to the levels of cell cultured with both ser/gly in the media (Figure 6D). In contrast, RCC cells cultured with glycine but without serine were not able to maintain cellular glutathione pools (Figure 6D). Cells cultured without either serine or glycine had even lower levels of glutathione. Using $^{13}C_3$ serine in concert with LC-MS/MS analysis, we examined if serine contributes directly to the GSH tripeptide. Label from serine contributed primarily to m+1 and m+2 pools of GSH (Figure S6C). Isotopic pattern analysis of the m+1 species demonstrated that serine contributes to the glycine moiety and to a lesser extent, the cysteine moiety (Figure S6D). Similar results were found upon analysis of the m+2 species (Figure S6E). These data are particularly relevant to tumor cells including RCC given that redox homeostasis is critical to maintaining proliferation. As exogenous serine is required to support proliferation of high L-2HG RCC cells, we considered if this was mediated through serine's support of GSH pools and redox homeostasis. We therefore examined the effects of buthionine sulphoximine (BSO) which blocks GSH synthesis via inhibition of γ-glutamylcysteine synthetase. BSO treatment led to a significant reduction in cellular glutathione pools despite the presence of serine in the media (Figure 6E). Furthermore, exogenous serine's promotion of RCC proliferation was diminished with BSO treatment (Figure 6F). Serine may also contribute to proliferation via purine biosynthesis through provision of one-carbon units and glycine. We therefore examined whether exogenous formate (to replenish one-carbon metabolism) and/or glycine could support proliferation in the absence of exogenous serine. In multiple high L-2HG RCC lines examined, formate plus glycine treatment could not rescue proliferation in the absence of serine (Supplemental Figure S6C).

Given these data, we next examined the impact of L-2HG on glutathione pools as a function of nutrient availability. Similar to parental cells, control vector (high L-2HG) cells demonstrated a

significant reduction of glutathione levels when cultured in the absence of serine (Figure 6G,H – compare lanes 1 and 2). In contrast, L2HGDH restored (low L-2HG) cells were able to maintain glutathione pools in the absence of exogenous serine (Figure 6G,H – compare lanes 3 and 4). We next examined the impact of L-2HG levels on the ability to withstand oxidative stress as a function of ser/gly availability. High L-2HG (control) 786-O RCC cells were sensitive (i.e. reduced viability) to ROS inducer t-butyl H_2O_2 upon ser/gly deprivation (Figure 6I- compare lanes 1 and 2). Similar findings were found in high L-2HG RCC cells expressing mutant L2HGDH (Figure 6I- compare lanes 5 and 6). In contrast, ser/gly deprivation did not sensitize WT L2HGDH-restored cells (low L-2HG) to t-butyl H_2O_2 (Figure 6I- compare lanes 3 and 4). Similar findings were found in 769p cells (Figure 6J). Next, we determined the relevance of dietary ser/gly on glutathione pools in vivo. 786-O xenografts in mice fed chow lacking ser/gly had lower total glutathione levels as compared with xenografts from mice fed chow replete with ser/gly (Figure 6K).

Translation relevance of raised L-2HG on serine metabolism.

These data prompted us to determine the translational relevance of our findings. We first analyzed the expression of serine biosynthetic genes in high L-2HG RCC, low L-2HG RCC, and normal kidney. L-2HG levels of samples is provided in Figure 7A. Consistent with prior studies, normal kidney tissues have low L-2HG level(5, 12, 26). High L-2HG RCC demonstrated reduced *PHGDH* mRNA expression as compared with both low L-2HG RCC and normal kidney (Figure 7B). Furthermore, high L-2HG RCC had lower expression of *PSAT1* mRNA than normal kidney (Figure 7C). Although low L-2HG RCC tumors trended toward lower *PSAT1* mRNA as compared with normal kidney, these data did not reach statistical significance. In agreement with these data, both PHGDH and PSAT1 protein expression is lower in high L-2HG RCC as compared with patient-matched adjacent uninvolved normal kidney (Figure 7D). Given our in vitro data demonstrating the importance of exogenous serine to the proliferation of high L-2HG RCC cells, we determined the relevance of this finding in vivo in mice fed chow +/- ser/gly. Similar to parental cells, the size of control vector (high L-2HG) OS-RC-2 xenografts is sensitive to dietary ser/gly deprivation (Figure 7E,compare lanes 1 and 2; and Figure S7). However, the size of L2HGDH restored xenografts was not affected by dietary ser/gly deprivation (Figure 7E,

compare lanes 3 and 4; and Figure S7). We next examined renal tissues from whole body *L2hgdh* knockout mice which we recently reported demonstrated elevated L-2HG levels and reduced L2HGDH protein (Figure 7F-G)(27). Kidneys from knockout mice demonstrated lower PHGDH protein expression (Figure 7H-I). We next determined serine levels from knockout and WT renal tissues. To exclude potential contribution from the diet, mice were fasted prior to renal harvest. As demonstrated in Figure 7J, serine levels are significantly lower in *L2hgdh* knockout kidneys as compared with kidneys from litter-mate WT mice.

DISCUSSION

We find that raised L-2HG levels results in a dependence on exogenous serine for renal tumor proliferation, in vivo growth, and redox homeostasis. To the best of our knowledge, this is the first report of a metabolic liability in the setting of high L-2HG. With the recognition that tumor cells have increased demands for nutrients including amino acids to support proliferation and biomass accumulation(28), there has been intense interest in identifying metabolic vulnerabilities that can be exploited. There has been particular focus on nonessential amino acids (NEAAs) as tumor cells often exhibit high demands for these nutrients that may outweigh their biosynthetic capacity. This has led to preclinical strategies including modified diets which serve as proof of principle that restricting an NEAA of interest may have therapeutic potential(29).

While dietary restriction of serine can suppress tumor growth in some preclinical models, others have proven resistant. Using isogenic cell lines, Maddocks *et al.* demonstrated that *p53* loss can sensitize colon cancer cells to dietary restriction of serine/glycine(30). Apart from this study, the underlying mechanisms that contribute to sensitivity (or resistance) to strategies that deplete serine are poorly understood. Accordingly, the tumor types most likely to benefit from such strategies remain largely unknown. A recent study demonstrated that human pancreatic ductal adenocarcinoma (PDAC), most of which harbor *KRAS* mutations, demonstrate loss of PHGDH expression and are therefore sensitive to deprivation of exogenous serine(31). However, the mechanism that drive this loss remain unclear. In addition, the metabolic sequelae of serine deprivation for tumor cells are highly context

dependent. For example, serine deprivation in low PHGDH PDAC tumor cells does not demonstrate appreciable effects on glutathione levels(31). In contrast, our studies reveal that exogenous serine is critical to maintain glutathione pools in RCC cells. Our findings are particularly relevant in light of multiple metabolomic data sets demonstrating that glutathione is among the most enriched metabolites in kidney cancer as compared with normal kidney(24, 25, 32). Notably, glycine alone cannot maintain glutathione pools in RCC cells. Our findings reveal that a major contribution of serine to glutathione pools in RCC is through transsulfuration. The rate-limiting step of this pathway generates cystathionine. In turn, cystathionine is converted to cysteine which can then incorporated into the glutathione tripeptide. Cysteine can also be generated from cystine which can be taken up by the xCT transporter system(33). However, the media conditions used throughout this study contained cystine indicating that the xCT system is not sufficient to generate the cysteine required for glutathione synthesis.

Our data reveal a dual mechanism by which serine biosynthetic enzymes are suppressed in RCC via remodeling of both the epigenome and epitranscriptome through the combined inhibition of histone demethylase KDM4C and the RNA m6A demethylases ALKBH5/FTO. KDM4C is known to require α-KG as a cofactor to promote amino acid biosynthetic/transport genes(13). However, the impact of an oncometabolite on the KDM4C-driven amino acid metabolism gene expression program has not been considered. m6A has previously been implicated in regulating ATF4. Zhou *et al.* proposed that ALKBH5 demethylation of a m6A site in the 5' region of the murine *Atf4* mRNA promotes translation(18). However, this m6A site is not conserved in humans suggesting the possibility that m6A regulation of ATF4 may be species-specific (34). Our data reveal a role for RNA methylation in regulating the serine biosynthetic enzyme gene *PSAT1*. Despite recent interest in m6A, most of the profiling studies to date do not provide single nucleotide resolution as they primarily depend on antibody-based pulldown approaches. Accordingly, the biologic significance of most m6A sites remains largely uncharacterized. Our data functionally validate the relevance of a m6A site in the direct regulation of an amino acid biosynthetic enzyme. Our data indicate that *PSAT1* m6A has post-transcriptional effects. Although m6A has been implicated in mRNA translation, the underlying mechanisms are poorly understood and warrant further study. Our studies reveal that L-2HG's effects

converge on serine biosynthetic enzyme expression through multiple regulatory levels (i.e. both histone and RNA methylation). Our data are the first to demonstrate loss of expression of multiple serine biosynthetic enzymes in a human cancer to the best of our knowledge.

Our findings present two key questions. First, how do high L-2HG RCCs meet their serine requirements? Our data reveal that diet is one potential source of serine for RCC tumors. An alternate consideration are endogenous sources of serine. The most relevant would be the kidney. A recent study analyzing metabolite exchange in pigs demonstrates that the kidney is a major contributor to systemic serine pools(35). These data are consistent with studies on isolated renal tubules from rats(36). Prior studies indicate that serine may generated from the *de novo* synthetic pathway that utilizes the glycolytic intermediate 3-phosphoglycerate as the starting substrate. An alternate pathway implicated in the kidney is the glycine cleavage system which can generate serine when coupled with serine hydroxymethyltransferases (SHMTs). Targeting these endogenous sources of systemic serine could represent a strategy to target tumors with suppressed serine biosynthetic enzyme expression as compared with strategies to deplete serine from the diet which may be more difficult to achieve in the clinic. The second question our findings raise is whether there is a benefit to loss of serine biosynthetic enzymes in RCC tumor cells? In addition to generating serine, the pathway generates other metabolites including α-KG. In fact, this pathway can be a major contributor to α-KG pools in embryonic stem cells(37). In the setting of RCC, α-KG generated during *de novo* serine biosynthesis would be expected to antagonize L-2HG's effects. Therefore, one theoretical advantage of suppressing this pathway is to maintain a higher ratio of L-2HG to α-KG. Future studies to investigate the potential advantage(s), if any, of suppressing this pathway in the context of L-2HG and other oncometabolites is warranted.

We recognize limitations of our study. Although our studies focused on serine, there may be alternate liabilities that ensue in the setting of high L-2HG. We also recognize that there may be additional mechanisms that cooperate with L-2HG to suppress serine biosynthetic enzyme expression in kidney cancer. RCC is known for low mutations burden. Hence, alternate epigenetic and/or epitranscriptomic mechanisms likely contribute to suppressed serine biosynthetic enzymes in RCC.

In summary, our studies reveal a metabolic liability that results from the dual activities of L-2HG on the epigenome and epitranscriptome. The combined analysis of our models, supported by our findings in patient tissues, demonstrates a dependence on exogenous serine in the setting of raised L-2HG. Our biochemical studies demonstrate that this renders high L-2HG kidney cancer cells dependent on exogenous serine to maintain cellular pools of glutathione, a key metabolite required for proliferation and redox homeostasis. Our findings provide novel mechanistic insight into metabolic rewiring induced by this metabolite. Accordingly, they provide rationale to purse strategies that limit serine availability for L-2HG driven kidney tumors.

METHODS

Sex as biologic variable. Our study examined male and female animals, and similar findings are reported for both sexes.

Cell culture. Renal cell lines were acquired from ATCC or NCI. OS-RC-2 cell line was acquired from RIKEN BioResource Research Center Cell Bank (https://cell.brc.riken.jp/en/). All cells were screened for Mycoplasma after their purchase. Cells are passaged for less than 3 months after resuscitation. All media were completed by adding 10% FBS (Atlanta biologicals #S11550) and 1X Penicillin-Streptomycin supplements (Fisher #MT30002CI). HEK293T was maintained in complete DMEM (4.5 gm glucose/lit) (Fisher #MT-10-017-CV) and all other cells were maintained in complete RPMI 1640 (Fisher #MT15040CM). For the studies that required serine/glycine deprivation, RPMI 1640 (Fisher #50-190-8105) was supplemented with 10% dialyzed FBS (Fisher #SH3007903), 1X Penicillin-Streptomycin, 30mg/lit L-Serine, 10 mg/lit glycine, 2 gm/lit glucose (Sigma #G7021), and 1X vitamin solution (Fisher #11120052).

Mice. CRISPR/cas9 mediated L2hgdh global knockout C57BL/6 mice were used in this study that we reported previously by Brinkley *et al*(27). Both male and female mice were used in this study. Mice were bred and maintained under specific pathogen-free conditions at University of Alabama at Birmingham following approved protocols. For in vivo xenograft studies, BALB/c Nude mice (strain code 194) were purchased from Charles River. All animals had *ad libitum* access to food and water and were maintained at 22–24 °C on a 12 hrs light/12 hrs dark cycle. For in vivo ser/gly restriction experiments, animals were

fed irradiated control ser/gly free chow obtained from Lab Animal Supplies Inc. Animals were observed daily for health status, and any mice that met IACUC criteria for euthanasia were immediately euthanized.

Chemicals and reagents. D-glucose U13C6, 99% (Cambridge Isotope Lab #CLM-1396-0.5); Tert-butyl hydroperoxide (Sigma #458139-100ML);Trizol (Life Technology #15596-018); RNA miniPrep (Zymo Research #R2052); High Capacity cDNA Synthesis Kit (Fisher #43-688-14); Taqman gene expression master mix (Fisher #43-690-16); SYBR Green master mix (Fisher #4367659); Blot stain Blue (Sigma #B-1177); 20X RNase free SSC (Thermo Scientific #AM9763); Nitrocellulose membrane (Biorad #1620112); PVDF membrane Immobilon-FL (Millipore # IPFL00010).

Plasmids and lentivirus. Plasmid DNAs for lentivirus productions were transfected to HEK-293T cells as described earlier(38). Supernatants from transfected HEK-293T cells were used to transduce target cells. Control vector, L2HGDH (wild type), and L2HGDH mutant (mutation at A241G) constructs were described previously(12). ATF4 (BC022088), PHGDH (BC000303), and PSAT1 (BC018129) cDNAs were purchased from transOMIC and placed into LV2606 backbone. Control (SHC016-1EA) and gene-targeted mission shRNAs in pLKO.1-puro backbone were purchased from Sigma: shMETTL3 (TRCN0000034717, TRCN0000289812, TRCN0000289814); shL2HGDH (TRCN0000064325, TRCN0000064326); shPHGDH (TRCN0000028501, TRCN0000233032). For CRISPR-Cas9 knockout (KO), lentiCRISPR-v2 (Addgene #52961) plasmid was linearized by BsmBI-v2 (NEB # R0739S), dephosphorylated, and gel-purified. Next, annealed oligos for L2HGDH-targeted (gRNA-3F, 3R) or control guide RNAs (Control_gRNA_F/R) were phosphorylated, ligated to the linearized plasmid, and propagated in *E.coli*. Control and targeted gRNAs used in this study are listed in supplementary Table S5. Plasmids were isolated and sequence-verified before use. Lentivirus-transduced cells were selected with puromycin.

GC/MS analysis of cellular L-2HG. Cells were briefly washed in ice-cold PBS, followed by rapid freezing in liquid nitrogen. Samples were added to pre-tared 2 ml screw cap tubes containing 1.4 mm ceramic beads, massed, and 800 µl of −20°C methanol with 2 µg/ml of both d4-succinic acid and disodium (R,S)-[2,3,3-2H3]-2-hydroxyglutarate ([2H3]-2HG) (C/D/N Isotopes, Canada) was added to the tubes. Samples were homogenized and incubated at −20°C for 1 h. Samples were then centrifuged to remove insoluble debris, and the supernatant dried in a vacuum centrifuge. The extract was then derivatized using a

previously described method to quantify D-2HG and L-2HG levels(39). Samples were injected into an Agilent 7890B/7250 GC-QTOF instrument (1:10 split ratio) equipped with a Phenomex ZB5-5 MSi column using a Gerstel MPS autosampler using previously described methods(40).Data were analyzed using MassHunter Qualitative Analysis and MassHunter Quantitative Analysis.

Mouse Tissue GC/MS. Mice were fasted for 6 hours before sacrifice and tissue isolation. Tissues were briefly washed in ice-cold in DPBS followed by rapid freezing in liquid nitrogen. GC/MS analysis was performed as previously described(40).

Tissue 2HG enantiomer analysis (i.e. D- and L-2HG quantification) by LC-MS/MS. Samples were analyzed as previously described(41). Briefly, enantiomer analyses were performed following derivatization with DATAN (diacetyl-L-tartaric acid followed by liquid chromatography-tandem mass spectrometry (LC-MS/MS) analysis and normalized to protein levels.

LC/MS preparation and method: 2 x 10^6 cells/10 cm culture plate were grown for 24 hrs in 7 ml RPMI 1640 (Teknova) supplemented with 10% dialyzed FBS (HyClone), 30 mg/L serine, 10 mg/L glycine, and 5.5 mM D-glucose. Cells were then thoroughly washed with DPBS and grown for 24 hrs in 7 ml RPMI 1640 (Teknova) supplemented with 10% dialyzed FBS, 30 mg/L serine, 10 mg/L glycine, and 5.5 mM (U-^{13}C6) D-glucose. Cells were then washed with ice cold 0.9% NaCl in molecular grade water and lysed in ice-cold 80% (v/v) LC-MS-grade methanol (Fisher). Lysed cells were scrapped into 1.5 ml microcentrifuge tube and stored in -80 °C. The cell lysate was spun at full speed (x16000g) for 20 minutes at 4 °C. Supernatant was isolated and dry vacuumed at room temperature until no liquid remained. The dry pellet was reconstituted into 30 ml solvent (water: methanol: acetonitrile; 2:1:1, v/v) and 3 μL was further analyzed by LC-MS.

Ultimate 3000 UHPLC (Dionex) is coupled to Q Exactive Plus-Mass spectrometer (QE-MS, Thermo Scientific) for metabolite profiling. A hydrophilic interaction chromatography method (HILIC) employing an Xbridge amide column (100 x 2.1 mm i.d., 3.5 μm; Waters) is used for polar metabolite separation. Detailed LC method was described previously (42) (43) except that mobile phase A was replaced with water containing 5 mM ammonium acetate (pH 6.8). The QE-MS is equipped with a HESI probe with related parameters set as below: heater temperature, 120 °C; sheath gas, 30; auxiliary gas,

10; sweep gas, 3; spray voltage, 3.0 KV for the positive mode and 2.5 kV for the negative mode; capillary temperature, 320 °C; S-lens, 55; scan range (m/z): 70 to 900 for positive mode (1.31 to 12.5 min) and negative mode (1.31 to 6.6 min) and 100 to 1000 for negative mode (6.61 to 12.5 min); resolution: 70000; automated gain control (AGC), 3×10^6 ions. Customized mass calibration was performed before data acquisition. LC/MS peak extraction and integration were performed using commercially available software Sieve 2.2 (Thermo Scientific). The peak area was used to represent the relative abundance of each metabolite in different samples. The missing values were handled as described in previous study (43).

LC-MS/MS analysis of Glutathione ^{13}C isotope incorporation: ~1 million 769P cells were maintained for 6 hrs in RPMI media containing 10% dialyzed FBS, 133 uM glycine, and no serine. Then $^{13}C_3$ labelled serine was added to the cells at a final concentration of 300 μM. 24 hrs later, the cells were washed once with ice-cold PBS and treated with ice-cold 80% methanol for 30 min to extract metabolites including glutathione. The extractions were centrifuged at 3000 x g for 10 min, and the supernatants were removed and dried to completion under nitrogen gas. The samples were then re-suspended in 100 μL of 0.1% formic acid in *dd*H_2O before LC-mass spectrometry analysis. An aliquot (20 μL) of each sample was loaded onto a 2.1 x 100 mm, 1.7 μm Luna Omega, 80 Å reverse-phase column (Phenomenex, Torrance, CA) at a flow rate of 400 μL/min A linear gradient of 5-50% mobile phase B for 10 min, then 50-98% B until 11 min with a 1 minute hold, then re-equilibration at initial conditions for 8 minutes using an Exion UHPLC (Sciex, Toronto, Ontario) and a flow rate of 100 μl/min was used. The mobile phases are A) ddH_2O with 0.1% formic acid and B) acetonitrile with 0.1% formic acid, respectively. The SCIEX 5600 Triple-Tof mass spectrometer (SCIEX, Toronto, Canada) was used to analyze the GSH ^{13}C profile. The IonSpray voltage for positive mode was 5500 V and the declustering potential was 100 V. Ionspray GS1/GS2 and curtain gases were both set at 40 psi. The interface heater temperature was 400°C. Eluted compounds were subjected to a time-of-flight survey scan from *m/z* 50-1000. Product ion time-of-flight scans for each possible ^{13}C incorporation of GSH were obtained to capture tandem mass spectra range from *m/z* 308.1-318.1, respectively, and were collected over 50 msec intervals using a collision energy spread of 10 V with a set collision point of 25 V. Spectra were centroided and de-isotoped by Analyst software, version 1.81 TF (Sciex, Toronto, Canada). LC-MS sample data were processed using

PeakView Software 2.2 (Sciex, Toronto, Ontario) to measure the GSH isotopic patterns and assess the ^{13}C incorporation sites using tandem mass spectrometry data collected for each via Product Ion Scans. ProteinProspector website (https://prospector.ucsf.edu/prospector/mshome.htm) was utilized to predict fragmentation patterns for the GSH-^{13}C incorporation.

***RT-qPCR and RNA sequencing*:** Total RNA from cultured cells or tissues were extracted using Trizol reagent (Invitrogen) and RNA miniPrep kit (Zymo Research). cDNA was synthesized using High-Capacity cDNA Reverse Transcription Kit (Thermo Scientific). Real time qPCR was performed using QuantStudio 6 flex (Thermo Scientific). For RNA sequencing from cell lines (RXF-control, RXF-L2HGDH), or tissues (normal kidney or low/high L-2HG kidney tumors), RNA were extracted followed by rRNA depletion. High-quality total RNA (RIN>7.0) were paired-end sequenced using Illumina HiSeq 2500 by Hudson Alpha Institute of Biotechnology, Huntsville, Alabama, USA (https://www.hudsonalpha.org/). After basecalls by Illumina bcl2fastq (v2.18.0.12), FASTQ files were aligned to GRCh37 (Release 25) reference genome assembly using STAR (v2.7.10a). Finally, transcript abundance was calculated using HTSeq-count (v2.0.2) and differential gene expression was analyzed by DESeq2.

Proliferation assays. Proliferating assay was either performed by cell counting using a hemocytometer or xCELLignece real-time cell analysis by ACEA Bioscinces (Agilent) as instructed by the company. Normalization was performed 24 hrs after cell attachment for both the methods.

Immunoblotting. For total cell lysates, cell pellet dissolved in DPBS containing 2% (w/v) SDS was sonicated briefly, centrifuged (16000g, 10 min, RT), and the supernatant was collected for analysis. Protein from whole cell lysates was quantified using a Pierce BCA Protein Assay Kit (Thermo Scientific). 10-20 ug lysates were resolved by 4-15% SDS-PAGE (Bio-Rad), transferred to PVDF membrane (Bio-Rad), and incubated with primary antibodies following standard protocols. Blots were developed using HRP-conjugated anti-rabbit (#45-000-683) or anti-mouse (#45-000-679) secondary antibodies (GE HealthCare) and HRP-substrate (Millipore # WBLUC0500). Primary antibodies used in this study are as follows: anti-L2HGDH (Genetex #GTX32695), anti-PHGDH (Cell Signaling #13428S), anti-β-actin (Abcam #ab20272), anti-PSAT1 (Proteintech #10501-1-AP), anti-ATF4 (Cell Signaling #11815S), anti-KDM4C (Novus #NB110-38884), anti-ALKBH5 (Cell Signaling #80283S), anti-FTO (Proteintech #27226-

1-AP), anti-ASNS (Proteintech #14681-1-AP), anti-Flag (Sigma #F1804), and anti-METTL3 (Cell Signaling #96391S).

siRNA gene knockdown. For siRNA-mediated gene knockdown, we followed the Lipofectamine RNAiMAX manufacturer's protocol (Thermo Scientific #13778150). Briefly, cells were seeded in a 6-well plate (200000 cells/well). After 24 hrs, the cells were treated with scrambled or gene-targeted siRNA constructs mixed with RNAiMax in reduced serum Opti-MEM medium (Thermo Scientific #31985070). 50-60 hrs after the treatment, cells were harvested for analysis. Details of siRNAs used in this study are listed in supplementary Table S5.

MTS assay. Cell viability upon exposure to oxidative stress was measured with a commercial cell viability MTS assay kit (Abcam #ab197010). Cells were grown in a 96-well plate and treated with 100 μM tert-Butyl H_2O_2 (Thermo Scientific) in designated media conditions for 8 hours and then assessed for viability following the kit protocol.

Xenograft. Cells were grown in RPMI media followed by trypsinization, washed 3x in DPBS with centrifugation in between. Cells were mixed in a 1:1 concentration with Matrigel (Corning #356234) and kept on ice until injection. Cells were injected in the flanks of immunocompromised mice. 1.5 million cells were injected in OS-RC-2 experiments and 3 million cells were injected for 786-O experiments. previously described(38).

ALKBH5 Assay. ALKBH5 enzymatic assay in the presence of L-2HG was assessed by a commercial ALKBH5 chemiluminescent assay kit (BPS Biosciences #79650) following the manufacturer's protocol. The luminescence signal was measured by GloMax navigator (Promega #GM2000).

Luciferase assay. pCAX human ATF4 5'-uORF plasmid was kindly provided by Dr. Takao Iwawaki (17). *Renilla* plasmid (pRL-SV40P) was a gift from Ron Prywes via Addgene(44). Cells were trypsinized and plated in HBSS with 10% dialyzed FBS for 4-8 hours before firefly luciferase and *Renilla* (internal control) measurements were taken using Promega Dual-Glo Luciferase Assay (Fisher).

Dot-blot. mRNAs was isolated from total RNA using Sigma/Roche mRNA isolation kit. mRNA concentration was measured using NanoDrop spectrophotometer (Thermo Scientific). mRNA was denatured at 65 °C for 15 min followed by chilling on ice immediately. mRNA was dotted on a

nitrocellulose membrane (BioRad). Once the membrane was dried, RNA was cross linked to the membrane using 120 mJoule/cm^2 density of UV light (UVP Hybrilinker HL-2000). Next, the membrane was washed once with 2X SSC solution (Thermo Scientific) and then incubated with 1X Blot Stain Blue (Sigma) for 1-2 minutes and then rinsed for several times with 1X TBST (Tris Buffer Saline pH 7.4, + 0.1% Tween 20) till the background blue was minimized. After imaging of the blue RNA dots, the membrane was blocked with 5% milk for 1 hr followed by overnight incubation with anti-m6A (Cell Signaling) antibody (1:1000 dilution) at 4 °C. After washing (3x), the membrane was incubated with HRP-conjugated anti-rabbit secondary antibody (GE HealthCare) for 1 hr (1:3000 dilution) and finally, the image was captured by a phosphoimager (Amersham, GE).

GSH measurements. Twenty hours after plating 300,000 cells in a six-well plate, media were changed to the corresponding experimental conditions. After 10 hours, cells were harvested and total glutathione pool (GSH + GSSG) were measured either using the protocol described previously (45) or using the protocol using the Thermo Fisher Glutathione Colorimetric Detection kit.

RNA immunoprecipitation, RT-qPCR, and m6A-sequencing. m6A-RNA immunoprecipitation was performed following the protocol provided by EpiMark N6-Methyladenosine Enrichment Kit (NEB #E1610S). Briefly, mRNA was isolated from total RNA following the manufacturer's protocol (Sigma #11741985001). ~250 ng mRNAs were subjected to restricted digestion using NEBNext Magnesium RNA Fragmentation Module (NEB #E6150S) (5 min, 94 °C). mRNA fragments were purified using RNA Clean and Concentrator Kit (Zymo Research #R1013). Then, the purified mRNA fragments were subjected to immunoprecipitation using m6A (Synaptic Systems) or control antibody-coated Protein G magnetic beads following the manufacturer's protocol. Immunoprecipitated mRNA fragments were purified, reverse transcribed, and analyzed by RT-qPCR using *PSAT1*-3'UTR-F1 and *PSAT1*-3'UTR-R1 primers. Details of the primers are listed in supplementary Table S5. m6A-RNA sequencing was performed by LC Sciences, Houston, Texas USA (https://lcsciences.com/) using their proprietary m6A-immunoprecipitation cut paired-end sequencing service using Illumina Novaseq6000 platform.

SELECT assay. For base-specific quantification of m6A-modification, SELECT assay was performed based on the protocol described by Xiao *et al.*(23). Briefly, a 17 μl reaction mix was set up in ice. The

mix contained total RNA (250 ng), SELECT Primer Up (40nM), SELECT Primer Down (40nM), dNTP (5uM), 1X NEB Cutsmart buffer (2μL), and H_2O. Each RNA is annealed to UP and Down primers for both the m6A and the control (-6bp) site. Annealing reaction was performed in a PCR machine (Thermo Scientific) as follows: 90 °C-2 mins, 80 °C-2 mins, 70 °C-2 mins, 60 °C-2 mins, 50°C-2 mins, 40 °C-12 mins, 4 °C-hold. Subsequently, a 3 μl enzyme mixture containing 0.01 U Bst 2.0 DNA polymerase (NEB), 0.5 U SplintR ligase (NEB), and 10 nmol ATP (NEB) was added to a final volume of 20 μl. The mixture was then incubated at 40 °C mins- 40 minutes, 80 °C-20 mins, and 4 °C-hold. 2 μL of this SELECT reaction was added to 8μL of RT-qPCR mix containing 5 μl SYBR Green PCR Master Mix (Thermo Scientific), 1 μl mix of SELECT qPCR-F and SELECT qPCR-R (200 nM), and 2 μl of nuclease free H_2O. RT-qPCR was run in QuantStudio 6 flex (Thermo Scientific). Relative m6A levels between experimental conditions was determined using the $1/^{\Delta\Delta}CT$ method. Details of the primers for the SELECT assay are listed in supplementary Table S5.

m6A-determination by LC-MS. Samples were prepared following the protocol described by Mathur *et al.* with some modifications(46). Briefly, 500 ng purified mRNAs from RCC cells were subjected to nuclease P1 (NEB) digestion in 35 μl reaction volume at 37 °C for 2 hrs, 2 μl of $ZnCl_2$ (stock 0.1 M) and 3 μl PCR grade H_2O were added to the digestion reaction to make up the volume to 40 μl. Next, 2 μl NH_4HCO3 (stock 2M) and 1 U alkaline phosphatase (Sigma) were added to the reaction and incubated for 2 hrs at 37 °C. Finally, 1 μl 1.2 M HCl was added to neutralize the solution. The samples were vortexed and then centrifuged for 30 mins at 16000g at 4 °C. The supernatants were collected. LC-MS analysis was used to quantify m6A and unmodified adenosine levels using standard curves generated for each nucleoside.

Statistics. Statistical analyses were carried out using GraphPad Prism-9 and SAS 9.4 software. Comparisons between groups for statistical significance were performed with a two tailed t-tests with a $p<0.05$ for significance unless otherwise specified. For multiple-group comparisons and repeated measures, ANOVA was performed with the indicated post hoc tests.

Study approval. All mouse studies were approved by the IACUC of The University of Alabama at Birmingham. Mice were maintained in standard care and were euthanized at predetermined experimental time points or at the first signs of morbidity according to the standards by the IACUC. All

human samples analyzed were acquired from the Cooperative Human Tissue Network and were provided to the investigators in a deidentified manner.

Data Availability. The published article includes all datasets generated or analyzed during this study. They are included in supplemental Table 1-4 and Supporting Data Values file. Sequencing data (RNAseq and m6Aseq) have been deposited in NCBI GEO (GSE228082).

Author Contributions. G.B., A.K., and S.S. participated in the conception, design of the study, and writing. H.D. and J.M. assisted with experimental design. A.K., G.B., H.N., S.K., E.S., H.W., J.L., Y.H., R.K., M.P., A.F., and N.M. acquired data. J.L., J.T., W.P., D.A., R.R., S.B., and D.C. assisted with data analysis. Co-first authorship order based on contribution to manuscript formatting. Declaration of interests: The authors declare no competing interests.

Acknowledgements. This work was supported by NIH R01CA200653 (to S.S.), F30CA232397 (to G.B.), NIH R01CA190429 (to H.D.), NIH R01CA236890 (to H.D.), Department of Veterans Affairs I01BX002930 (to S.S), and P30CA013148 (S.S., S.B., R.R.). A.K was supported in part by a Research Scholar Award from the Urology Care Foundation (Award No.669279) and a Concept Award from the Department of Defense (Award No. HT9425-23-1-0339). This work was supported in part by UAB Nathan Shock Center P30 AG050886. We would also like to acknowledge the assistance of the Comprehensive Genomics and Transgenic Animal Shared Facilities at the O'Neal Comprehensive Cancer Center and the Targeted Metabolomics and Proteomics Laboratory (TMPL) at UAB. We thank Dianna Xing, Michelle Johnson, and Victor Darley-Usmar for assistance with glutathione measurements and Sagnik Giri (University of Arizona) for assistance with manuscript formatting.

References

1. Pollard PJ, Briere JJ, Alam NA, Barwell J, Barclay E, Wortham NC, et al. Accumulation of Krebs cycle intermediates and over-expression of HIF1alpha in tumours which result from germline FH and SDH mutations. *Human molecular genetics.* 2005;14(15):2231-9.
2. Dang L, White DW, Gross S, Bennett BD, Bittinger MA, Driggers EM, et al. Cancer-associated IDH1 mutations produce 2-hydroxyglutarate. *Nature.* 2009;462(7274):739-44.
3. Yan H, Parsons DW, Jin G, McLendon R, Rasheed BA, Yuan W, et al. IDH1 and IDH2 mutations in gliomas. *N Engl J Med.* 2009;360(8):765-73.
4. Ward PS, Patel J, Wise DR, Abdel-Wahab O, Bennett BD, Coller HA, et al. The common feature of leukemia-associated IDH1 and IDH2 mutations is a neomorphic enzyme activity converting alpha-ketoglutarate to 2-hydroxyglutarate. *Cancer Cell.* 2010;17(3):225-34.
5. Shim EH, Livi CB, Rakheja D, Tan J, Benson D, Parekh V, et al. L-2-Hydroxyglutarate: an epigenetic modifier and putative oncometabolite in renal cancer. *Cancer Discov.* 2014;4(11):1290-8.
6. Xu W, Yang H, Liu Y, Yang Y, Wang P, Kim SH, et al. Oncometabolite 2-hydroxyglutarate is a competitive inhibitor of alpha-ketoglutarate-dependent dioxygenases. *Cancer Cell.* 2011;19(1):17-30.
7. Smith EH, Janknecht R, and Maher LJ, 3rd. Succinate inhibition of alpha-ketoglutarate-dependent enzymes in a yeast model of paraganglioma. *Human molecular genetics.* 2007;16(24):3136-48.
8. Lu C, Ward PS, Kapoor GS, Rohle D, Turcan S, Abdel-Wahab O, et al. IDH mutation impairs histone demethylation and results in a block to cell differentiation. *Nature.* 2012;483(7390):474-8.
9. Xiao M, Yang H, Xu W, Ma S, Lin H, Zhu H, et al. Inhibition of alpha-KG-dependent histone and DNA demethylases by fumarate and succinate that are accumulated in mutations of FH and SDH tumor suppressors. *Genes & development.* 2012;26(12):1326-38.
10. Isaacs JS, Jung YJ, Mole DR, Lee S, Torres-Cabala C, Chung YL, et al. HIF overexpression correlates with biallelic loss of fumarate hydratase in renal cancer: novel role of fumarate in regulation of HIF stability. *Cancer Cell.* 2005;8(2):143-53.
11. McBrayer SK, Mayers JR, DiNatale GJ, Shi DD, Khanal J, Chakraborty AA, et al. Transaminase Inhibition by 2-Hydroxyglutarate Impairs Glutamate Biosynthesis and Redox Homeostasis in Glioma. *Cell.* 2018;175(1):101-16 e25.
12. Shelar S, Shim EH, Brinkley GJ, Kundu A, Carobbio F, Poston T, et al. Biochemical and Epigenetic Insights into L-2-Hydroxyglutarate, a Potential Therapeutic Target in Renal Cancer. *Clin Cancer Res.* 2018;24(24):6433-46.
13. Zhao E, Ding J, Xia Y, Liu M, Ye B, Choi JH, et al. KDM4C and ATF4 Cooperate in Transcriptional Control of Amino Acid Metabolism. *Cell reports.* 2016;14(3):506-19.
14. Lu PD, Harding HP, and Ron D. Translation reinitiation at alternative open reading frames regulates gene expression in an integrated stress response. *J Cell Biol.* 2004;167(1):27-33.
15. Vattem KM, and Wek RC. Reinitiation involving upstream ORFs regulates ATF4 mRNA translation in mammalian cells. *Proceedings of the National Academy of Sciences of the United States of America.* 2004;101(31):11269-74.
16. Hinnebusch AG. The scanning mechanism of eukaryotic translation initiation. *Annual review of biochemistry.* 2014;83:779-812.
17. Iwawaki T, Akai R, Toyoshima T, Takeda N, Ishikawa TO, and Yamamura KI. Transgenic mouse model for imaging of ATF4 translational activation-related cellular stress responses in vivo. *Scientific reports.* 2017;7:46230.
18. Zhou J, Wan J, Shu XE, Mao Y, Liu XM, Yuan X, et al. N(6)-Methyladenosine Guides mRNA Alternative Translation during Integrated Stress Response. *Molecular cell.* 2018;69(4):636-47 e7.
19. Liu J, Yue Y, Han D, Wang X, Fu Y, Zhang L, et al. A METTL3-METTL14 complex mediates mammalian nuclear RNA N6-adenosine methylation. *Nat Chem Biol.* 2014;10(2):93-5.
20. Zheng G, Dahl JA, Niu Y, Fedorcsak P, Huang CM, Li CJ, et al. ALKBH5 is a mammalian RNA demethylase that impacts RNA metabolism and mouse fertility. *Molecular cell.* 2013;49(1):18-29.
21. Jia G, Fu Y, Zhao X, Dai Q, Zheng G, Yang Y, et al. N6-methyladenosine in nuclear RNA is a major substrate of the obesity-associated FTO. *Nat Chem Biol.* 2011;7(12):885-7.
22. Linder B, Grozhik AV, Olarerin-George AO, Meydan C, Mason CE, and Jaffrey SR. Single-nucleotide-resolution mapping of m6A and m6Am throughout the transcriptome. *Nat Methods.* 2015;12(8):767-72.

23. Xiao Y, Wang Y, Tang Q, Wei L, Zhang X, and Jia G. An Elongation- and Ligation-Based qPCR Amplification Method for the Radiolabeling-Free Detection of Locus-Specific N(6) -Methyladenosine Modification. *Angew Chem Int Ed Engl.* 2018;57(49):15995-6000.
24. Hakimi AA, Reznik E, Lee CH, Creighton CJ, Brannon AR, Luna A, et al. An Integrated Metabolic Atlas of Clear Cell Renal Cell Carcinoma. *Cancer Cell.* 2016;29(1):104-16.
25. Li B, Qiu B, Lee DS, Walton ZE, Ochocki JD, Mathew LK, et al. Fructose-1,6-bisphosphatase opposes renal carcinoma progression. *Nature.* 2014;513(7517):251-5.
26. Wang H, Wang L, Zheng Q, Lu Z, Chen Y, Shen D, et al. Oncometabolite L-2-hydroxyglurate directly induces vasculogenic mimicry through PHLDB2 in renal cell carcinoma. *International journal of cancer.* 2021;148(7):1743-55.
27. Brinkley G, Nam H, Shim E, Kirkman R, Kundu A, Karki S, et al. Teleological role of L-2-hydroxyglutarate dehydrogenase in the kidney. *Dis Model Mech.* 2020;13(11).
28. Hosios AM, Hecht VC, Danai LV, Johnson MO, Rathmell JC, Steinhauser ML, et al. Amino Acids Rather than Glucose Account for the Majority of Cell Mass in Proliferating Mammalian Cells. *Developmental cell.* 2016;36(5):540-9.
29. Maddocks ODK, Athineos D, Cheung EC, Lee P, Zhang T, van den Broek NJF, et al. Modulating the therapeutic response of tumours to dietary serine and glycine starvation. *Nature.* 2017;544(7650):372-6.
30. Maddocks OD, Berkers CR, Mason SM, Zheng L, Blyth K, Gottlieb E, et al. Serine starvation induces stress and p53-dependent metabolic remodelling in cancer cells. *Nature.* 2013;493(7433):542-6.
31. Banh RS, Biancur DE, Yamamoto K, Sohn ASW, Walters B, Kuljanin M, et al. Neurons Release Serine to Support mRNA Translation in Pancreatic Cancer. *Cell.* 2020;183(5):1202-18 e25.
32. Bansal A, Sanchez DJ, Nimgaonkar V, Sanchez D, Riscal R, Skuli N, et al. Gamma-Glutamyltransferase 1 Promotes Clear Cell Renal Cell Carcinoma Initiation and Progression. *Mol Cancer Res.* 2019;17(9):1881-92.
33. Sato H, Tamba M, Ishii T, and Bannai S. Cloning and expression of a plasma membrane cystine/glutamate exchange transporter composed of two distinct proteins. *J Biol Chem.* 1999;274(17):11455-8.
34. Boulias K, Toczydlowska-Socha D, Hawley BR, Liberman N, Takashima K, Zaccara S, et al. Identification of the m(6)Am Methyltransferase PCIF1 Reveals the Location and Functions of m(6)Am in the Transcriptome. *Molecular cell.* 2019;75(3):631-43 e8.
35. Neinast MD, Jang C, Hui S, Murashige DS, Chu Q, Morscher RJ, et al. Quantitative Analysis of the Whole-Body Metabolic Fate of Branched-Chain Amino Acids. *Cell metabolism.* 2019;29(2):417-29.e4.
36. Lowry M, Hall DE, and Brosnan JT. Serine synthesis in rat kidney: studies with perfused kidney and cortical tubules. *Am J Physiol.* 1986;250(4 Pt 2):F649-58.
37. Hwang IY, Kwak S, Lee S, Kim H, Lee SE, Kim JH, et al. Psat1-Dependent Fluctuations in alpha-Ketoglutarate Affect the Timing of ESC Differentiation. *Cell metabolism.* 2016;24(3):494-501.
38. Kundu A, Nam H, Shelar S, Chandrashekar DS, Brinkley G, Karki S, et al. PRDM16 suppresses HIF-targeted gene expression in kidney cancer. *J Exp Med.* 2020;217(6).
39. Gibson KM, ten Brink HJ, Schor DS, Kok RM, Bootsma AH, Hoffmann GF, et al. Stable-isotope dilution analysis of D- and L-2-hydroxyglutaric acid: application to the detection and prenatal diagnosis of D- and L-2-hydroxyglutaric acidemias. *Pediatr Res.* 1993;34(3):277-80.
40. Li H, and Tennessen JM. Preparation of Drosophila Larval Samples for Gas Chromatography-Mass Spectrometry (GC-MS)-based Metabolomics. *J Vis Exp.* 2018(136).
41. Rakheja D, Boriack RL, Mitui M, Khokhar S, Holt SA, and Kapur P. Papillary thyroid carcinoma shows elevated levels of 2-hydroxyglutarate. *Tumour Biol.* 2011;32(2):325-33.
42. Liu X, Sadhukhan S, Sun S, Wagner GR, Hirschey MD, Qi L, et al. High-Resolution Metabolomics with Acyl-CoA Profiling Reveals Widespread Remodeling in Response to Diet. *Mol Cell Proteomics.* 2015;14(6):1489-500.
43. Liu X, Ser Z, and Locasale JW. Development and quantitative evaluation of a high-resolution metabolomics technology. *Anal Chem.* 2014;86(4):2175-84.
44. Chen X, and Prywes R. Serum-induced expression of the cdc25A gene by relief of E2F-mediated repression. *Mol Cell Biol.* 1999;19(7):4695-702.
45. Tietze F. Enzymic method for quantitative determination of nanogram amounts of total and oxidized glutathione: applications to mammalian blood and other tissues. *Anal Biochem.* 1969;27(3):502-22.

46. Mathur L, Jung S, Jang C, and Lee G. Quantitative analysis of m(6)A RNA modification by LC-MS. *STAR Protoc.* 2021;2(3):100724.

Main Figure Legend

Figure 1. High L-2HG suppresses amino acid synthesis and transporter genes in RCC.

A) Differentially expressed transcripts in RXF-393 control vector (high L-2HG) relative to cells transduced with L2HGDH cDNA (low L-2HG). Amino acid synthesis and transporter genes are indicated (horizontal dotted line denotes p-value of 0.05).

B) Relative mRNA of *PHGDH* and *PSAT1* (normalized to RPLPO) from RXF-393 cells stably expressing either control (black) vector or L2HGDH (red). Data are mean ± SD from n=4 biological replicates.

C, D) Relative mRNA levels of amino acid synthetic/transporter genes from 769p (C) and 786-O (D) cells stably expressing the indicated construct. Expression was normalized to RPLPO. Data are mean ± SD from n=4 biological replicates. *p<0.05, **p<0.005, ***p<0.0001.

E) Immunoblot of PHGDH, PSAT1, and L2HGDH protein from 769p and 786-O transduced with either control vector or L2HGDH cDNA. Actin (β-actin) or Ponceau S stain was used as the loading control. Blots are from the same biologic sample run contemporaneously.

F) Immunoblot of ASNS protein from 786-O and OS-RC-2 RCC cells transduced with control vector or L2HGDH cDNA. Actin was used as the loading control.

G, H) Immunoblot of RXF-393 (G) and 769p (H) cells stably expressing either control vector, L2HGDH (WT), or L2HGDH A241G (catalytic mutant). Actin was used as the loading control.

I) Tandem-MS analysis for L-2HG and D-2HG metabolites from control (black) or L2HGDH KO (red) HK2 renal epithelial cells normalized to protein content. Data are mean ± SEM from n=3 biological replicates.

J) mRNA expression of the indicated genes was examined by qRT-PCR from Control (black) or L2HGDH KO (red) HK2 cells. Data are expressed as mean ± SEM from n=3 biological replicates. *p<0.05, **p<0.005.

K) Immunoblot for PHGDH protein from HK2 cells treated with either DMSO or L-2HG octyl ester (5 mM) or DMOG (1 mM) for 4 hrs. Actin was used as the loading control.

Figure 2. L-2HG suppression of ATF4.

A) Immunoblot for ATF4 protein from 786-O, OS-RC-2, and 769p RCC cells stably transduced with the indicated vectors. Actin was used as the loading control.

B) Immunoblot for ATF4 protein from 786-O cells stably transduced with control vector, L2HGDH (WT), or L2HGDH A241G (mutant). Actin was used as the loading control.

C) Immunoblot for L2HGDH and ATF4 protein from control and L2HGDH KO HK2 cells. Actin was used as the loading control.

D) Immunoblot for ATF4 and PHGDH from 769p cells stably expressing either control vector or ATF4 cDNA. Actin was used as the loading control.

E) Relative ATF4 mRNA (normalized to TBP) was examined by qRT-PCR from 769p and 786-O cells stably expressing either control (black) vector or L2HGDH cDNA (red). Data are expressed as mean ± SD from n=3 (769p) or n=4 (786-O) biological replicates.

F, G) 786-O (F) and A498 (G) cells stably transduced with L2HGDH cDNA were transiently transfected (55 hrs) with either scramble siRNA (Scr) or siRNAs targeting KDM4C (#1, #2). Immunoblotting for KDM4C, ATF4, PHGDH, and PSAT1 was performed. Actin (β-actin) or tubulin (α-tubulin) was used as the loading control.

H) Upper panel represents the construct containing the human ATF4 5'-uORFs preceding firefly luciferase. Lower panel: relative luciferase signal following transient transfection of the luciferase construct into 769p and 786-O cells stably expressing the indicated vector (control vector [black], L2HGDH WT [red], or L2HGDH A141G mutant [blue]). Data are normalized to Renila-luc. Data are presented as mean ± SEM. ANOVA was used, and the Tukey's post-hoc p-values are provided in figure.

Figure 3. L-2HG promotes mRNA m6A methylation in RCC.

A, B) m6A dot blot of 100 ng of mRNA isolated from 786-O (A) and 769p (B) cells (n=3, biological replicates) stably expressing either control vector or L2HGDH (WT). Methylene blue blot serves as loading control.

C) Quantification of m6A normalized to methylene blue as shown in A and B. Data are mean ± SD from n=3 biological replicates.

D) LC-MS/MS analysis of m6A levels in mRNA from RXF-393 cells stably expressing control vector or L2HGDH. Data are presented as a ratio of m6A to unmodified adenosine (m6A/A). Data are mean ± SD from n=4 biological replicates.

E) m6A dot blot of mRNA isolated from RXF-393 cells stably expressing either control vector, L2HGDH (WT), or L2HGDH mutant (A241G).

F) In vitro ALKBH5 activity with increasing concentration of L-2HG. Each data point represents mean ± error values of n=2 technical replicates.

G) 786-O cells stably transduced with L2HGDH cDNA were transiently treated with either scramble siRNA (Scr) or siRNAs targeting ALKBH5 and FTO (52 hrs). mRNA was harvested and assess for m6A via dot blot.

H) Volcano plot of m6A-seq demonstrating relative changes in m6A peaks in mRNAs isolated from high (control) vs low (L2HGDH transduced) L2HG 786-O cells (n=1, each). Red denotes higher m6A levels in high L-2HG levels. Blue denotes lower m6A levels in high L-2HG levels.

I) m6A-Seq analysis of the *PSAT1* mRNA from 786-O control (high L-2HG) and L2HGDH (low L-2HG) cells. For each condition, enrichment is displayed as RNA m6A immunoprecipitated (RIP) normalized to the corresponding input.

J) m6A-IP qRT-PCR was used to assess m6A enrichment in the *PSAT1* 3'UTR from 786-O cells stably transduced with the indicated vector. PSAT1-1F/1R primer pair was used. Data are represented as mean ± SD from n=3 biological replicates.

Figure 4. Regulation of PSAT1 expression through L-2HG induced m6A.

A, B) Immunoblot of METTL3 and PSAT1 from 769p (A) and 786-O (B) cells stably expressing the indicated shRNA (shC= control shRNA). Actin/ponceau serve as loading control. Relative PSAT1 was normalizing to ponceau.

C) qRT-PCR analysis of *PSAT1* mRNA expression (normalized to RPLPO) from 786-O and 769p cells stably expressing control shRNA (shC) or METTL3 targeting shRNA. Data are represented as mean ± SD from n=3 biological replicates.

D) Immunoblot of ALKBH5 and PSAT1 from HK2 renal epithelial cells transiently transfected (52 hrs) with scramble siRNA (Scr) or siRNAs targeting ALKBH5 (#1, #2, and #3). Relative PSAT1 was determined by normalizing to ponceau loading control.

E, F) Immunoblot of ALKBH5 and PSAT1 from 786-O/L2HGDH (E) and 769p/L2HGDH (F) cells transiently transfected (52 hrs) with the indicated siRNA (scramble siRNA= Scr). Relative PSAT1 was normalized to ponceau.

G) Immunoblot of FTO and PSAT1 from 769p/L2HGDH cells transiently transfected (52 hrs) with the indicated siRNA. Relative PSAT1 are normalized to ponceau.

H, I, J) Relative m6A by SELECT at the GGACT site within the *PSAT1* 3'-UTR. In panel H, relative m6A in 786-O cells transduced with control shRNA (shC) or shMETTL3. Panels I and J demonstrate relative m6A levels in 786-O (I) and 769p (J) cells transduced with vector control or L2HGDH. Data are mean ± SD from n=3 biological replicates.

K, L) 769p were stably transduced with FLAG-tagged PSAT1 (WT) construct. Cells were transiently transfected (52 hrs) with the indicated siRNA followed by immunoblotting (panel K). Panel L is quantitative densitometry of FLAG levels normalized to Actin. Data are represented as mean ± SD from n=3 biological replicates. ANOVA was used, and the Tukey's post-hoc p-values are provided in figure.

M) 769p were stably transduced with FLAG-tagged PSAT1 (Mut) construct. Cells were transiently transfected (52 hrs) with the indicated siRNA followed by immunoblotting.

Figure 5. High L2HG causes exogenous serine dependency in RCC cell lines.

A) LC-MS analysis of serine synthesis (m+3) from labeled glucose [U-13C]. Data are mean ± SD from n=6 biological replicates.

B) Proliferation of OSRC-2 stably transduced with the indicated vector (left panel- control; right panel-L2HGDH) in media with or without Ser/Gly. Data are mean ± SD from n=3 biological replicates. Repeated measures analysis was conducted, and the p-values reflect Tukey's post-hoc comparisons.

C, D) Relative growth ratio (-SerGly/+SerGly) at day 4 in RCC cells transduced with the indicated vector. Data are mean ± SD from n=3 biological replicates. *$p<0.05$.

E) Immunoblot of PHGDH from 769p cells stably expressing either control vector or PHGDH cDNA.

F, G) Proliferation of 769p cells transduced with control vector (E) or PHGDH (F) in media +/- SerGly. Data are mean ± SD from n=3 biological replicates of each group. Repeated measures analysis was conducted, and the p-values reflect Tukey's post-hoc comparisons.

H) Immunoblot of Sn12pm6 cells stably expressing the indicated shRNA.

I) Relative L/D-2HG levels in Sn12pm6 cells transduced with the indicated shRNAs (shC = control). Data are mean ± SEM from n=3 biological replicates.

J, K) Cell proliferation (by connectivity index) was measured from Sn12pm6-Scr (J) and Sn12pm6-shL2HGDH (K) cells grown +/- SerGly. Data are mean ± SD from n=4 biological replicates of each group. Repeated measures analysis was conducted, and the p-values reflect Tukey's post-hoc comparisons.

L) OS-RC-2 cells were subcutaneously implanted. After implantation, mice were randomly distributed and fed chow +/- SerGly (n=10, each group) for four weeks (left panel). Tumor volume at day 28 is provided in the right panel. Data are mean ± SEM. Repeated measures analysis was performed followed by Tukey's post-hoc comparisons at each time point.

M) 786-O xenografts were established in flanks of nude mice. After the average tumor size reached 100 mm^3, mice were fed chow +/- SerGly (n=7, each group) and followed over time (left panel). Xenograft size (day 40) is provided in the right panel. Data are mean ± SEM. Repeated measures analysis was performed followed by Tukey's post-hoc comparisons at each time point.

Figure 6. Exogenous serine is required for glutathione synthesis in RCC.

A) Principal component plot from partial least squares discriminant analysis (PLS-DA) of metabolites from 769p cells grown in media containing either both serine and glycine, glycine only, or no serine and glycine (none). (n=5 biological replicates per group).

B) LC-MS analysis of metabolites extracted from the three groups of 769p cells described in panel A.

C) Schematic view of serine and glycine incorporation into glutathione (GSH).

D) Analysis of cellular glutathione levels from 769p cells cultured for 24 hrs in media as indicated. Results are presented as mean ± SEM from n=4 biological replicates of each group. ANOVA p-value <0.0001. Post-hoc Tukey's p-values are provided in figure.

E) Analysis of cellular glutathione levels from 769p cells cultured for 24 hrs in serine-containing media +/- BSO. Data are presented as mean ± SD from n=3 biological replicates per group. **p<0.005

F) Cell proliferation as determined by connectivity index in 769p cells grown as indicated. Each data point is presented as mean ± SD from n=4 biological replicates of each group.

G, H) Glutathione levels of 786-O (G) and 769p (H) cells stably expressing control vector or L2HGDH and cultured for 24 hrs in media with or without (none) Ser. Data are mean ± SEM from n=3 biological replicates in each group. *p<0.05, **p<0.005, ns=not significant.

I, J) Relative fraction of viable cells in 786-O (I) and 769p (J) cells stably expressing the indicated vector and treated with 100 □M tert-butyl H2O2 for 24 hrs in the presence/absence of SerGly. Results are presented as mean ± SEM from n=3 biological replicates of each group. *p<0.05, **p<0.005, ***p<0.0001.

K) Quantification of the glutathione content in the 786-O xenografts in mice fed chow +/- SerGly. Xenografts are from data presented in Fig. 5P. The result is presented as mean ± SEM. *p<0.05.

Figure 7. Translational relevance of raised L-2HG in RCC.

A) LC-MS analysis of L-2HG content (normalized to total protein content) from patient tissues harvested from either normal kidneys (black), high L2HG tumors (red dots), or low L2HG tumors (blue dots). Data are presented as mean ± SEM from n=9 samples. Data were analyzed by one-way ANOVA followed by post hoc Tukey's honestly significant difference test. ANOVA p-value is <0.0001 (F =18.54). Post hoc analysis p-values are demonstrated in the figures.

B, C) mRNA expression of *PHGDH* (B) and *PSAT1* (C) from the samples in panel A. Data are presented as mean ± SEM. Data were analyzed by one-way ANOVA followed by post hoc Tukey's honestly significant difference test. ANOVA p-values for (B) and (C) are 0.0002 (F =12.91) and 0.0932 (F=2.624), respectively. Post hoc analysis p-values are demonstrated in the figures.

D) Immunoblot analysis of PHGDH and PSAT1 from patient-matched (n=3) high L2HG tumors and adjacent normal kidney. Third panel PHGDH western is from same blot with shorter exposure time.

E) Relative tumor size of OSRC-2 xenografts (+/- L2HGDH) at 4 weeks in mice fed chow +/- SerGly. After average tumor size reached 100 mm^3, mice were randomly distributed into two groups (n=8, each group). Data are mean ± SEM.

F, G) Immunoblot of L2HGDH protein (F) and densitometric quantification (G) in renal cortical tissue from WT and L2HGDH KO (global) mice. Data normalized to Actin. Data presented in panel G as mean ± SEM.

H, I) PHGDH immunoblot and quantification from the WT and L2HGDH KO mouse renal cortical tissues. Data normalized to Actin. Data presented in panel I are mean ± SEM.

J) GC-MS analysis of serine from WT and global L2HGDH KO renal cortical tissues. Data presented as mean ± SEM from n=7 mice in each group.

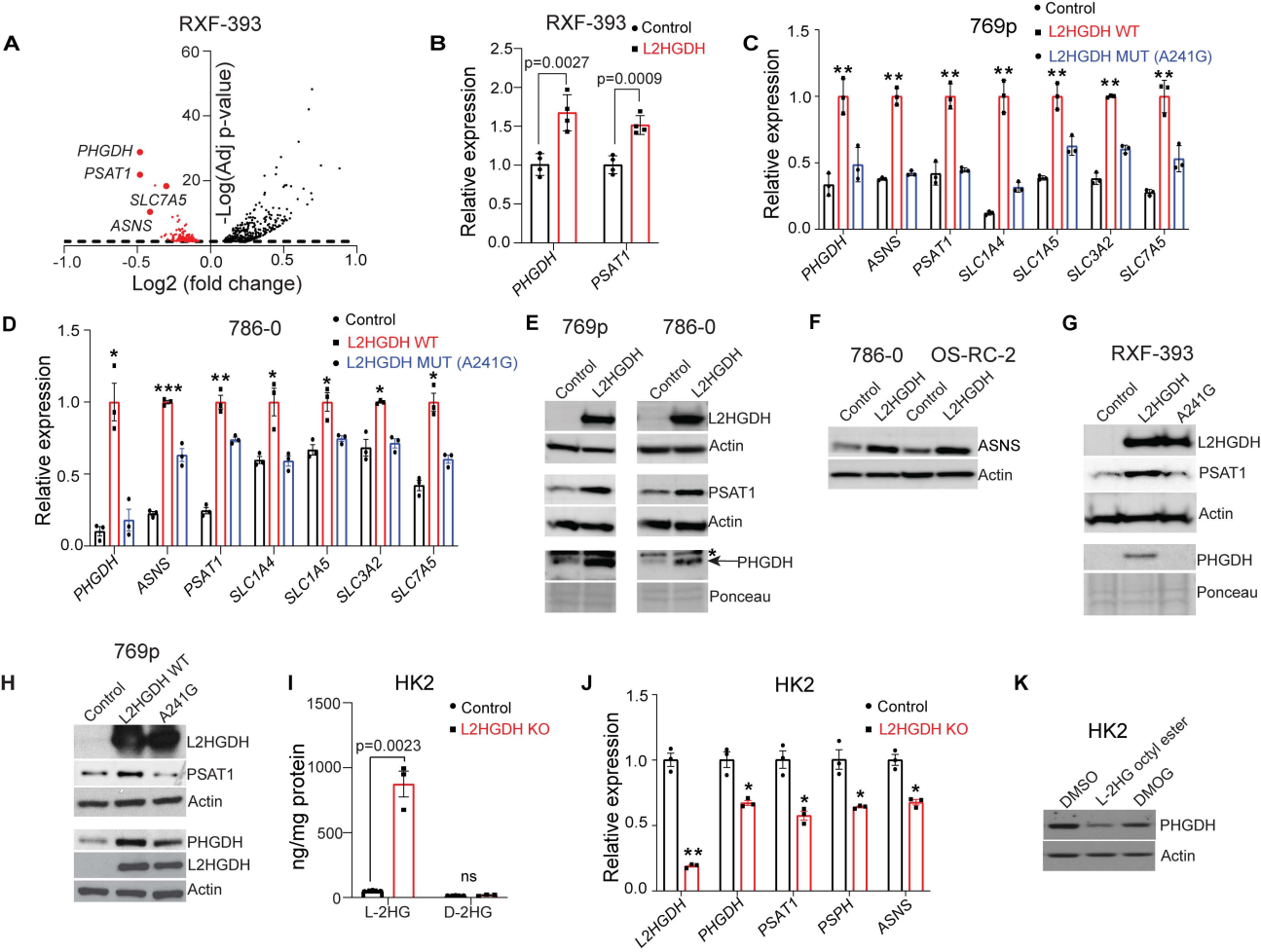
A
RXF-393
-Log(Adj p-value)
Log2 (fold change)
PHGDH
PSAT1
SLC7A5
ASNS
B
RXF-393
Control
L2HGDH
Relative expression
p=0.0027
p=0.0009
PHGDH
PSAT1
C
769p
Control
L2HGDH WT
L2HGDH MUT (A241G)
Relative expression
PHGDH
ASNS
PSAT1
SLC1A4
SLC1A5
SLC3A2
SLC7A5
D
786-0
Control
L2HGDH WT
L2HGDH MUT (A241G)
Relative expression
PHGDH
ASNS
PSAT1
SLC1A4
SLC1A5
SLC3A2
SLC7A5
E
769p
786-0
Control
L2HGDH
L2HGDH
Actin
PSAT1
Actin
PHGDH
Ponceau
F
786-0
OS-RC-2
Control
L2HGDH
Control
L2HGDH
ASNS
Actin
G
RXF-393
Control
L2HGDH
A241G
L2HGDH
PSAT1
Actin
PHGDH
Ponceau
H
769p
Control
L2HGDH WT
A241G
L2HGDH
PSAT1
Actin
PHGDH
L2HGDH
Actin
I
HK2
Control
L2HGDH KO
ng/mg protein
p=0.0023
ns
L-2HG
D-2HG
J
HK2
Control
L2HGDH KO
Relative expression
L2HGDH
PHGDH
PSAT1
PSPH
ASNS
K
HK2
DMSO
L-2HG octyl ester
DMOG
PHGDH
Actin

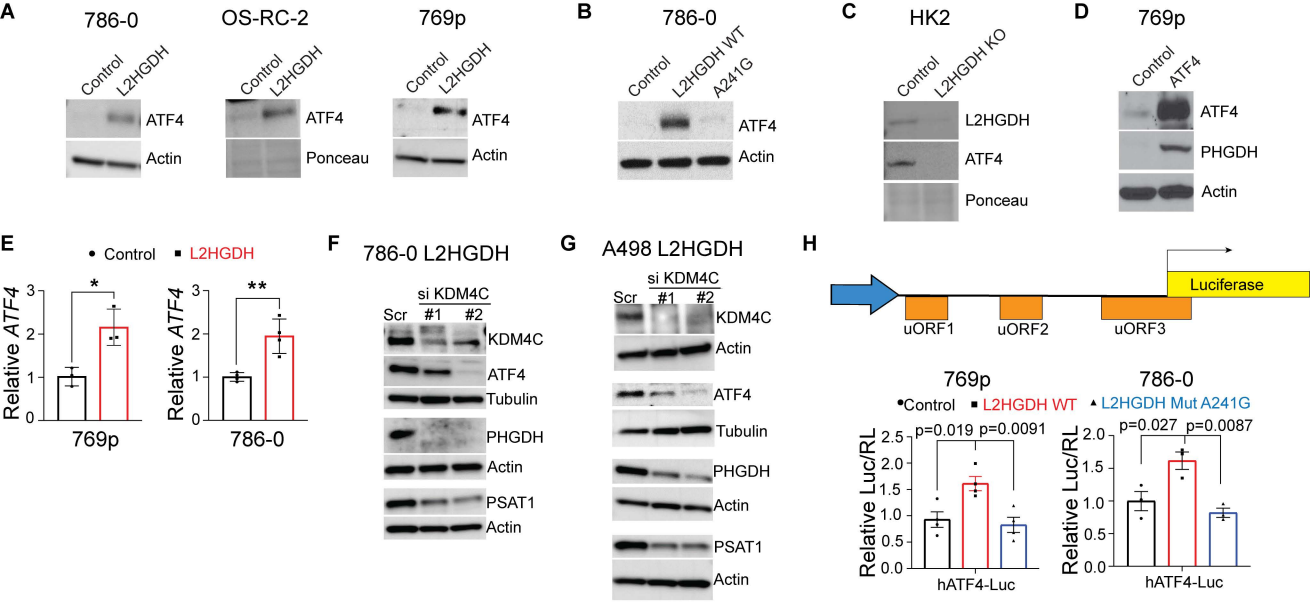
A
786-0
OS-RC-2
769p
Control
L2HGDH
ATF4
Actin
Ponceau
B
786-0
L2HGDH WT
A241G
C
HK2
L2HGDH KO
L2HGDH
D
769p
PHGDH
E
Control
L2HGDH
Relative ATF4
769p
786-0
F
786-0 L2HGDH
si KDM4C
Scr
#1
#2
KDM4C
Tubulin
PHGDH
PSAT1
G
A498 L2HGDH
H
Luciferase
uORF1
uORF2
uORF3
L2HGDH WT
L2HGDH Mut A241G
p=0.019
p=0.0091
p=0.027
p=0.0087
Relative Luc/RL
hATF4-Luc

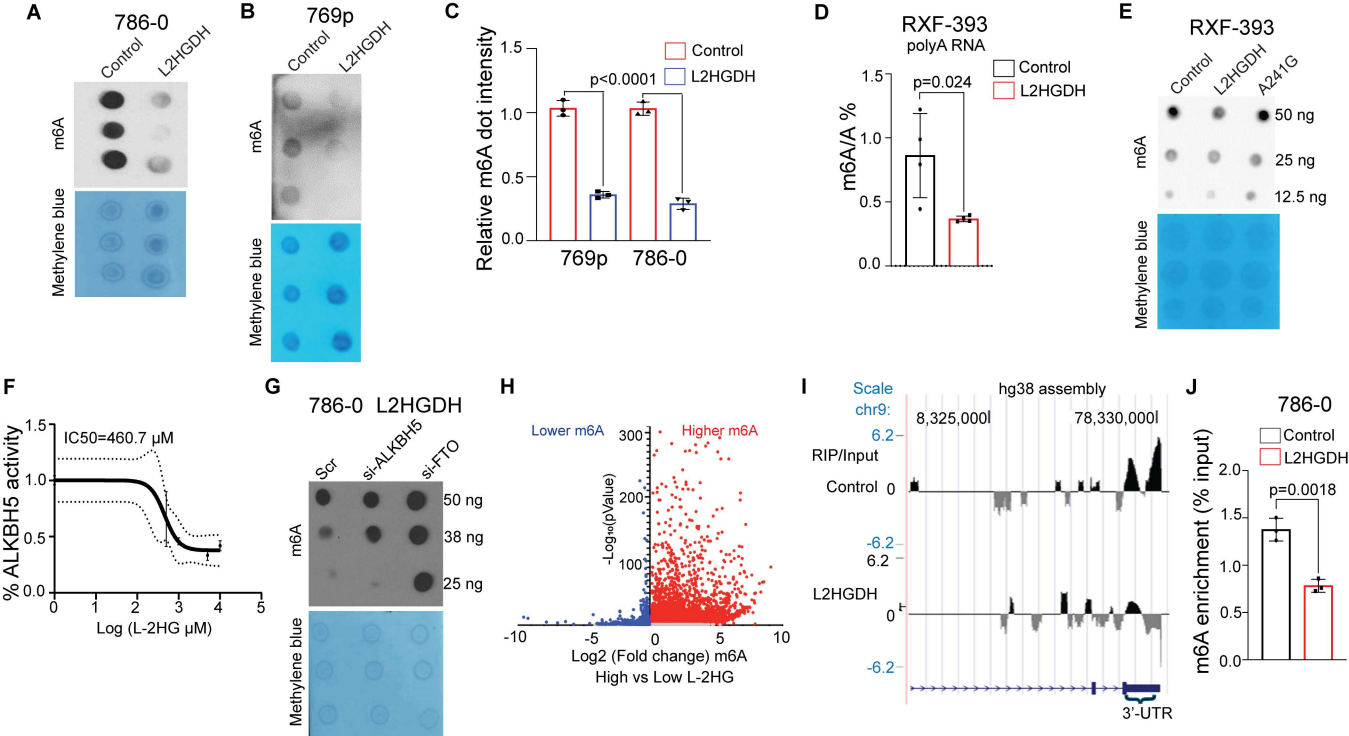
A
786-0
Control
L2HGDH
m6A
Methylene blue
B
769p
Control
L2HGDH
m6A
Methylene blue
C
Relative m6A dot intensity
1.5
1.0
0.5
0.0
p<0.0001
Control
L2HGDH
769p
786-0
D
RXF-393
polyA RNA
m6A/A %
1.5
1.0
0.5
0.0
p=0.024
Control
L2HGDH
E
RXF-393
Control
L2HGDH
A241G
m6A
50 ng
25 ng
12.5 ng
Methylene blue
F
% ALKBH5 activity
1.5
1.0
0.5
0.0
IC50=460.7 μM
0
1
2
3
4
5
Log (L-2HG μM)
G
786-0 L2HGDH
Scr
si-ALKBH5
si-FTO
m6A
50 ng
38 ng
25 ng
Methylene blue
H
Lower m6A
Higher m6A
-Log10(pValue)
300
200
100
-10
-5
0
5
10
Log2 (Fold change) m6A
High vs Low L-2HG
I
Scale
chr9:
8,325,000l
78,330,000l
hg38 assembly
6.2
RIP/Input
Control
0
-6.2
6.2
L2HGDH
0
-6.2
3'-UTR
J
786-0
Control
L2HGDH
m6A enrichment (% input)
2.0
1.5
1.0
0.5
0.0
p=0.0018

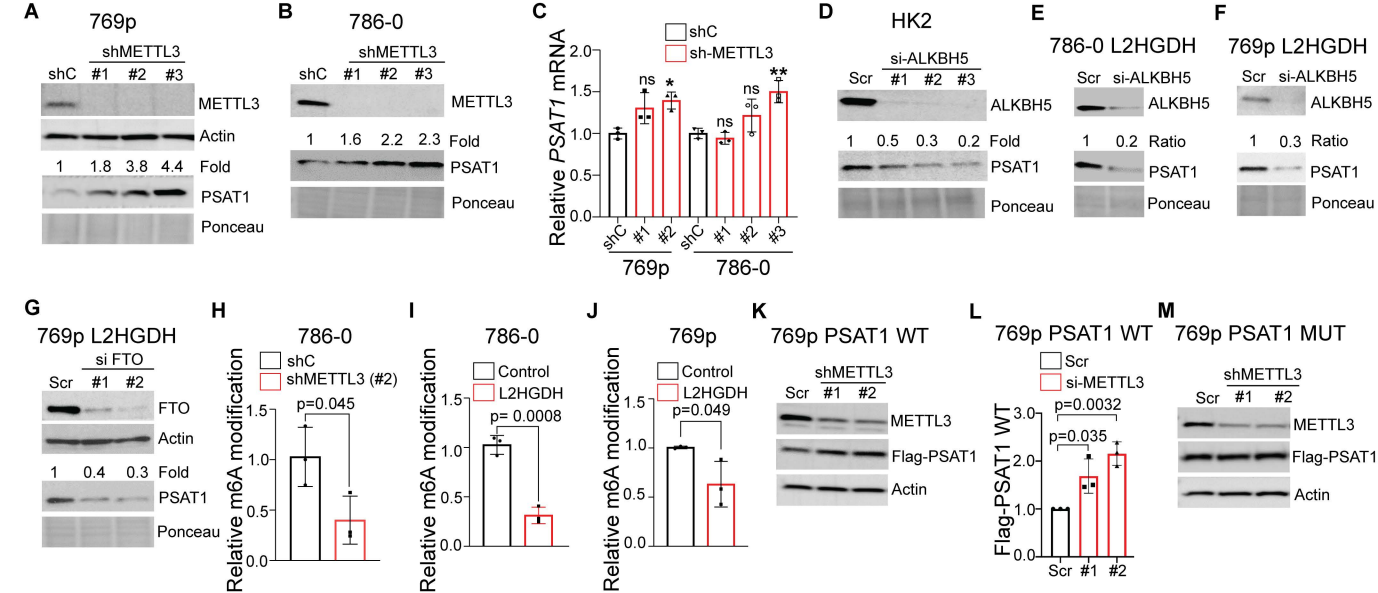
A
769p
shMETTL3
shC #1 #2 #3
METTL3
Actin
1 1.8 3.8 4.4 Fold
PSAT1
Ponceau
B
786-0
shMETTL3
shC #1 #2 #3
METTL3
1 1.6 2.2 2.3 Fold
PSAT1
Ponceau
C
shC
sh-METTL3
Relative PSAT1 mRNA
ns
*
ns
ns
**
shC #1 #2 shC #1 #2 #3
769p
786-0
D
HK2
si-ALKBH5
Scr #1 #2 #3
ALKBH5
1 0.5 0.3 0.2 Fold
PSAT1
Ponceau
E
786-0 L2HGDH
Scr si-ALKBH5
ALKBH5
1 0.2 Ratio
PSAT1
Ponceau
F
769p L2HGDH
Scr si-ALKBH5
ALKBH5
1 0.3 Ratio
PSAT1
Ponceau
G
769p L2HGDH
si FTO
Scr #1 #2
FTO
Actin
1 0.4 0.3 Fold
PSAT1
Ponceau
H
786-0
shC
shMETTL3 (#2)
Relative m6A modification
p=0.045
I
786-0
Control
L2HGDH
Relative m6A modification
p= 0.0008
J
769p
Control
L2HGDH
Relative m6A modification
p=0.049
K
769p PSAT1 WT
shMETTL3
Scr #1 #2
METTL3
Flag-PSAT1
Actin
L
769p PSAT1 WT
Scr
si-METTL3
Flag-PSAT1 WT
p=0.0032
p=0.035
Scr #1 #2
M
769p PSAT1 MUT
shMETTL3
Scr #1 #2
METTL3
Flag-PSAT1
Actin

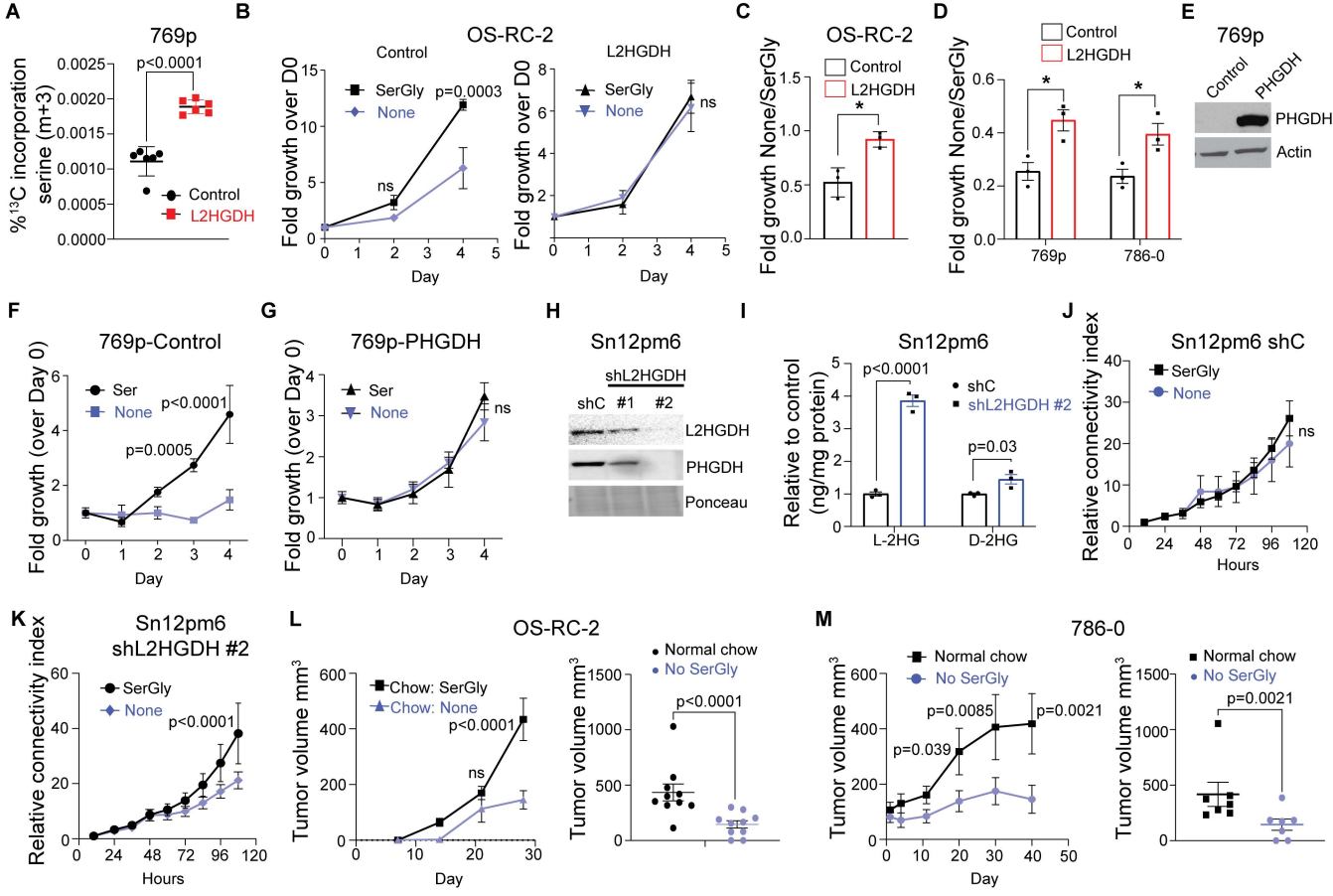
A
769p
p<0.0001
%13C incorporation serine (m+3)
Control
L2HGDH
B
OS-RC-2
Control
L2HGDH
SerGly
None
p=0.0003
ns
Fold growth over D0
Day
C
OS-RC-2
Control
L2HGDH
Fold growth None/SerGly
D
Control
L2HGDH
769p
786-0
E
769p
Control
PHGDH
PHGDH
Actin
F
769p-Control
Ser
None
p<0.0001
p=0.0005
Fold growth (over Day 0)
Day
G
769p-PHGDH
Ser
None
ns
H
Sn12pm6
shL2HGDH
shC #1 #2
L2HGDH
PHGDH
Ponceau
I
Sn12pm6
p<0.0001
p=0.03
shC
shL2HGDH #2
Relative to control (ng/mg protein)
L-2HG
D-2HG
J
Sn12pm6 shC
SerGly
None
ns
Relative connectivity index
Hours
K
Sn12pm6 shL2HGDH #2
SerGly
None
p<0.0001
Relative connectivity index
Hours
L
OS-RC-2
Chow: SerGly
Chow: None
p<0.0001
ns
Tumor volume mm3
Day
Normal chow
No SerGly
p<0.0001
M
786-0
Normal chow
No SerGly
p=0.0085
p=0.0021
p=0.039
Tumor volume mm3
Day
p=0.0021

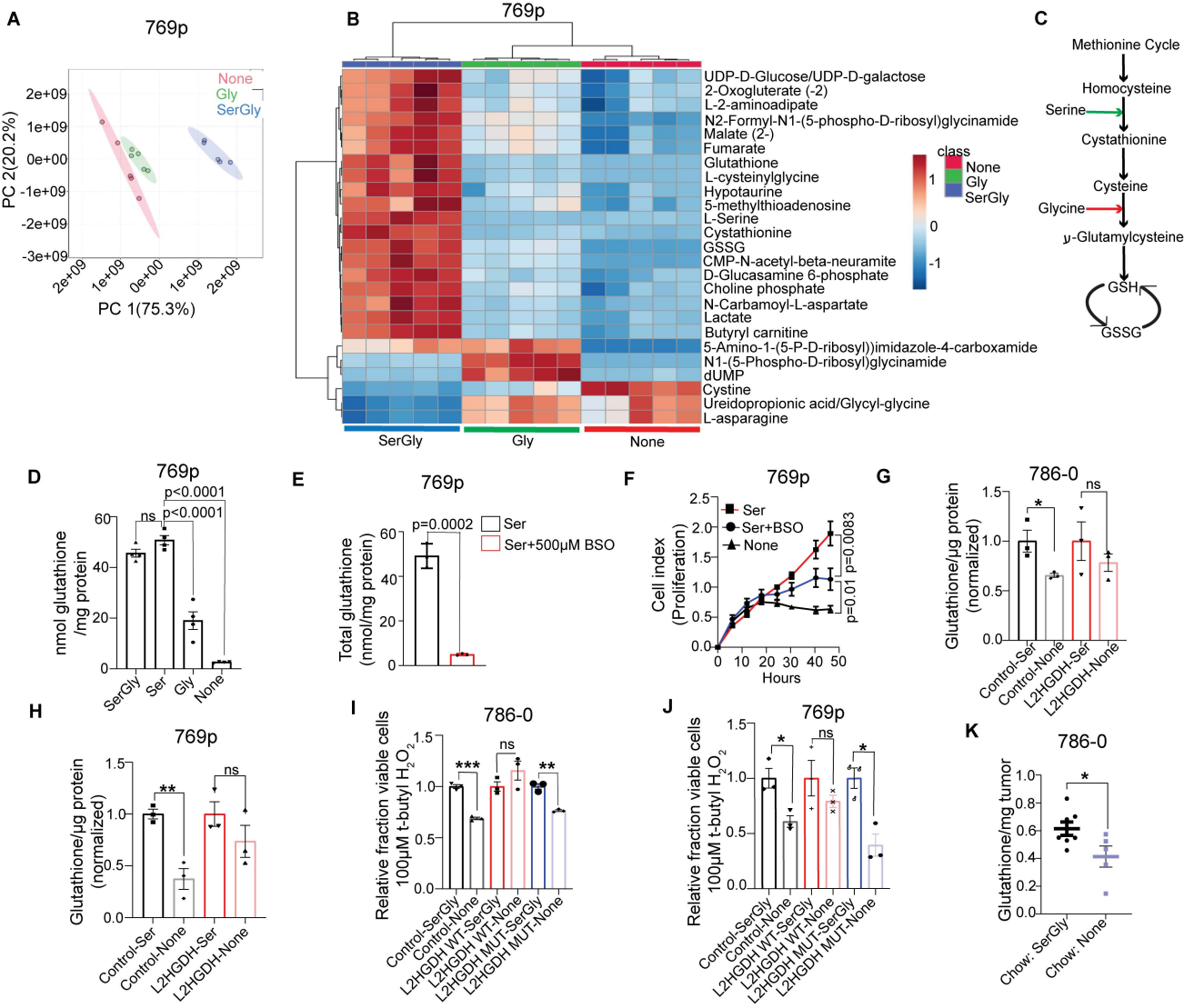
A
769p
None
Gly
SerGly
PC 2(20.2%)
PC 1(75.3%)
B
769p
UDP-D-Glucose/UDP-D-galactose
2-Oxogluterate (-2)
L-2-aminoadipate
N2-Formyl-N1-(5-phospho-D-ribosyl)glycinamide
Malate (2-)
Fumarate
Glutathione
L-cysteinylglycine
Hypotaurine
5-methylthioadenosine
L-Serine
Cystathionine
GSSG
CMP-N-acetyl-beta-neuramite
D-Glucasamine 6-phosphate
Choline phosphate
N-Carbamoyl-L-aspartate
Lactate
Butyryl carnitine
5-Amino-1-(5-P-D-ribosyl))imidazole-4-carboxamide
N1-(5-Phospho-D-ribosyl)glycinamide
dUMP
Cystine
Ureidopropionic acid/Glycyl-glycine
L-asparagine
class
None
Gly
SerGly
SerGly
Gly
None
C
Methionine Cycle
Homocysteine
Serine
Cystathionine
Cysteine
Glycine
γ-Glutamylcysteine
GSH
GSSG
D
769p
nmol glutathione /mg protein
p<0.0001
p<0.0001
ns
SerGly
Ser
Gly
None
E
769p
Total glutathione (nmol/mg protein)
p=0.0002
Ser
Ser+500μM BSO
F
769p
Cell index (Proliferation)
Ser
Ser+BSO
None
p=0.01 p=0.0083
Hours
G
786-0
Glutathione/μg protein (normalized)
ns
Control-Ser
Control-None
L2HGDH-Ser
L2HGDH-None
H
769p
Glutathione/μg protein (normalized)
ns
Control-Ser
Control-None
L2HGDH-Ser
L2HGDH-None
I
786-0
Relative fraction viable cells
100μM t-butyl H_2O_2
ns
Control-SerGly
Control-None
L2HGDH WT-SerGly
L2HGDH WT-None
L2HGDH MUT-SerGly
L2HGDH MUT-None
J
769p
Relative fraction viable cells
100μM t-butyl H_2O_2
ns
Control-SerGly
Control-None
L2HGDH WT-SerGly
L2HGDH WT-None
L2HGDH MUT-SerGly
L2HGDH MUT-None
K
786-0
Glutathione/mg tumor
Chow: SerGly
Chow: None

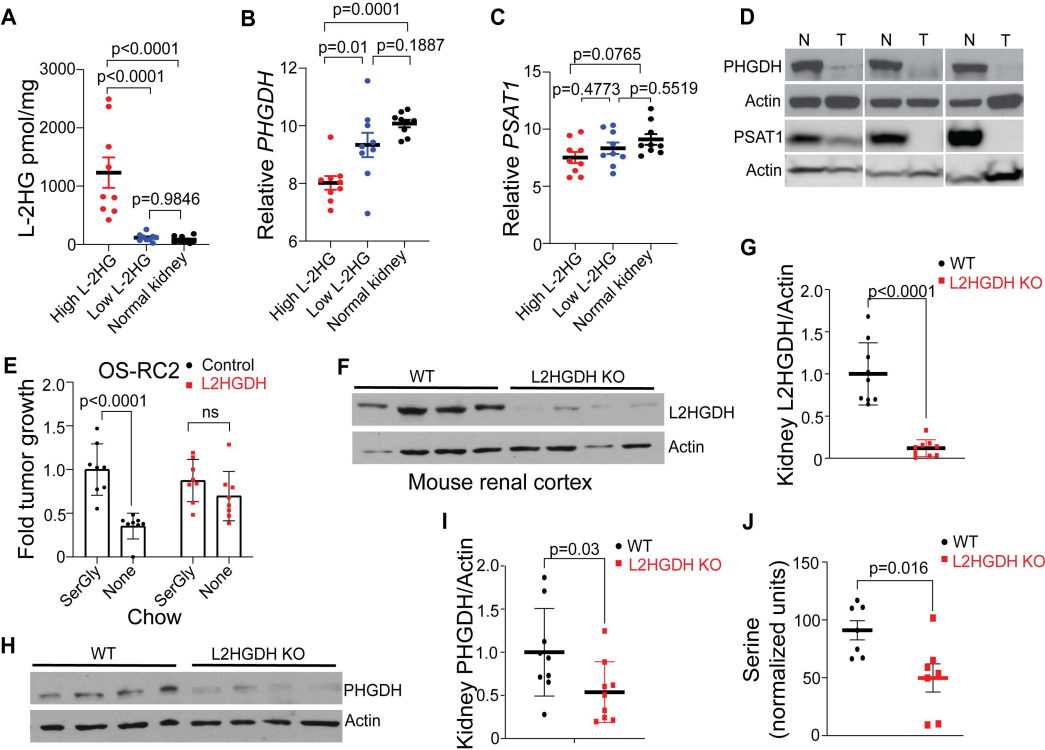
A
L-2HG pmol/mg
3000
2000
1000
0
p<0.0001
p<0.0001
p=0.9846
High L-2HG
Low L-2HG
Normal kidney
B
Relative PHGDH
12
10
8
6
p=0.0001
p=0.01
p=0.1887
High L-2HG
Low L-2HG
Normal kidney
C
Relative PSAT1
15
10
5
p=0.0765
p=0.4773
p=0.5519
High L-2HG
Low L-2HG
Normal kidney
D
N T N T N T
PHGDH
Actin
PSAT1
Actin
E
OS-RC2
Control
L2HGDH
Fold tumor growth
2.0
1.5
1.0
0.5
0
p<0.0001
ns
SerGly
None
SerGly
None
Chow
F
WT
L2HGDH KO
L2HGDH
Actin
Mouse renal cortex
G
WT
L2HGDH KO
Kidney L2HGDH/Actin
2.0
1.5
1.0
0.5
0
p<0.0001
H
WT
L2HGDH KO
PHGDH
Actin
I
Kidney PHGDH/Actin
2.0
1.5
1.0
0.5
0
p=0.03
WT
L2HGDH KO
J
Serine
(normalized units)
150
100
50
0
p=0.016
WT
L2HGDH KO